Nuclear Physics B351 (1991) 507–560
North-Holland

QCD CORRECTIONS TO HEAVY QUARK PRODUCTION IN HADRON–HADRON COLLISIONS

W. BEENAKKER* and W.L. VAN NEERVEN

Instituut Lorentz, University of Leiden, P.O.B. 9506, 2300 RA Leiden, The Netherlands

R. MENG** and G.A. SCHULER***

II Institut für Theoretische Physik, Universität Hamburg, W-2000 Hamburg 50, Germany

J. SMITH

Institute for Theoretical Physics, State University of New York at Stony Brook, NY 11794-3840, USA

Received 11 June 1990
(Revised 7 September 1990)

We investigate the QCD corrections to the cross section and single-particle inclusive differential distributions for $p + \bar{p} \to Q(\overline{Q}) + X$ where Q and $\overline{Q}$ are heavy quarks. We calculate the order α_s corrections to the parton reaction $q + \bar{q} \to Q + \overline{Q}$ which involves the computation of the virtual gluon contributions and the soft and hard contributions from the reaction $q + \bar{q} \to Q + \overline{Q} + g$. The contributions from the channels $g + q(\bar{q}) \to Q + \overline{Q} + q(\bar{q})$ are also calculated. Including the order α_s corrections to $g + g \to Q + \overline{Q}$ from our previous paper we give exact results for the order α_s^3 cross sections and single-particle inclusive differential distributions for the production of t and b quarks in $p\bar{p}$ collisions at energies presently available at the CERN $Sp\bar{p}S$ and the Fermilab tevatron. Results for future pp colliders are also presented. Finally we compare the results of the simple approximations to the order α_s corrections with the exact results.

1. Introduction

The subject of this paper is heavy flavour production in single-particle inclusive hadron–hadron processes

$$H_1 + H_2 \to Q(\overline{Q}) + X, \tag{1.1}$$

* Supported by the Stichting F.O.M.
** Supported by LAA, CERN, Geneva.
*** Supported by the Bundesministerium für Forschung und Technologie, 05 4HH 92P/3, Bonn, Germany.

0550-3213/91/$03.50 © 1991 – Elsevier Science Publishers B.V. (North-Holland)

where H_i denote the hadrons, $Q(\overline{Q})$ the heavy quarks such as c, b and t and X stands for any hadronic final state. In lowest order the heavy flavour production is described by the following parton–parton processes [1]

$$q + \bar{q} \to Q + \overline{Q}, \tag{1.2}$$

and

$$g + g \to Q + \overline{Q} \tag{1.3}$$

The first and second process are known as quark–antiquark annihilation and gluon–gluon fusion, respectively Recently the order α_S corrections to (1 2) and (1.3) have been calculated [2, 3]. These include all the virtual corrections to (1 2) and (1.3) as well as the contributions from the bremsstrahlung reactions

$$q + \bar{q} \to Q + \overline{Q} + g, \tag{1.4}$$

$$g + g \to Q + \overline{Q} + g, \tag{1.5}$$

$$g + q(\bar{q}) \to Q + \overline{Q} + q(\bar{q}). \tag{1.6}$$

The work reported here is part of a series of papers. In ref. [4] we presented the calculation of the order α_S QCD corrections to the heavy flavour production cross sections and single-particle inclusive differential distributions from the gluon–gluon channel (1.3) and our results agreed with those published in ref [2] We have now completed the calculations for the other two channels (1 2) and (1.6), and therefore finished a completely independent calculation of the exact order α_S corrections to (1.1).

There are several reasons for doing this Theoretical predictions for reaction (1.1) are used to set limits on the mass of the top quark [5–7] They are also used to understand lepton signals from $b(\bar{b})$ semileptonic decays, yielding both experimental distributions for $b(\bar{b})$ production [8], as well as backgrounds in the search for new physics. These experimental tests confirm the predictive power of perturbative QCD. Finally the contributions from (1.3) give us information on the behaviour of the gluon structure function, which plays an important role in predicting cross sections for future accelerators It is therefore very important to know that the complete order α_S corrections to (1 2) and (1 3) have been calculated correctly.

Our results for the corrections to the parton–parton cross sections (1.2) and (1.3) agree numerically with those reported in ref. [2]. Hence we also agree with their predictions for hadron–hadron cross sections. We have also checked numerically that both calculations agree on the single-particle inclusive differential spectra of the heavy quark in rapidity and transverse momentum in the parton–parton collisions. We would like to thank P. Nason for his help in making these checks There are, however, small differences between some of our results and those in ref. [3] for the hadron–hadron differential spectra. These are not caused by differences at the parton–parton level and will be commented on in due course. Since the details of the work in refs. [2,3] have never been published we have written up our calculation in some detail so that it complements the write-up in ref. [4].

The paper is also a continuation of an investigation begun in ref. [9], which was a study of simple approximations to the complicated formulae for the higher order corrections. The reason for such work can be summarized as follows. First, the actual calculations of the various distributions in heavy flavour production [2–4] show that the order α_S corrections are large. It is now common to describe QCD corrections by a so-called K-factor which in this case ranges from 2–3 depending on which heavy flavour is produced. Since the order α_S calculation is so involved it is unlikely that exact corrections beyond this order will be computed. Second, some approximations and their resummations are used in current Monte Carlo programs [10–12]. A comparison between the exact and approximate distributions gives an indication of the usefulness of these programs.

The construction of approximate formulae will clearly only be successful if the theoretical and experimental uncertainties are so large that the differences between the exact and the approximate corrections will hardly be distinguishable. Further, the approximation has to contain all terms which dominate the order α_S correction. Moreover, it has to be generalized to higher orders. This approach works very well in the case of the Drell–Yan vector boson production $p + \bar{p} \to V + X$ [13], in radiative W-boson production $p + \bar{p} \to W + \gamma + X$ [14] and in direct photon production $p + \bar{p} \to \gamma + X$ [15]. However, in the case of heavy flavour production this approach does not work so well as far as the total cross sections are concerned [9]. This can mainly be attributed to the fact that in the latter case the K-factor on the parton level shows too much structure contrary to what we observed for the three processes mentioned above. The reason for this will be explained below.

A thorough analysis reveals that the corrections to (1.2) and (1.3) are dominated by the following production mechanisms [3,9]: initial state soft gluon bremsstrahlung (ISGB), flavour excitation (FE) and gluon splitting (GS). The first mechanism (ISGB) accounts for the threshold behaviour whereas the latter two explain the high-energy behaviour of the parton–parton cross section. A fourth mechanism is represented by the final state quark fragmentation (FSQF). However it turns out that the latter is rather small for the whole range of energies and we will not discuss it anymore. Initial state gluon bremsstrahlung occurs in processes (1.4) and (1.5) whereas gluon splitting and flavour excitation show up in (1.5) and (1.6). However the above mechanisms fail to explain the behaviour of the parton–parton cross section at medium energies [9], for instance $\eta = s/4m^2 - 1$ values $0.1 < \eta < 10$, where m denotes the heavy quark mass and $\sqrt{s}$ is the total parton–parton c.m.

energy. In this region all parton cross sections show a dip which can even become negative. Unfortunately this region gives very important contributions to the hadronic total cross section when the parton cross section is convoluted with the total parton flux The consequence is that in most cases the approximate order α_S hadronic cross section exceeds the exact one by 20–40% [9] In this paper we examine the differential distributions to see whether one gets reasonable agreement between the exact and approximate expressions in specific regions of phase space. This is possible since we have completed our independent calculation of the order α_S corrections to (1.2) and (1 3)

The paper is organized as follows. In sects. 2 and 3 we present the calculation of the QCD process (1.6) and corrections to reaction (1 2) which involves the computation of the cross section for the channel (1 4). We follow the procedure in ref. [4] In sect 4 we perform the mass factorizations on the cross sections in two different schemes, i e. $\overline{\mathrm{MS}}$ and DIS. Sect 5 is devoted to a discussion of the parton–parton cross sections and differential distributions. It is at this stage that we can check our results with the plots in ref [2] and with results from their computer program. In sect 6 we present our exact results for the heavy quark differential distributions in the reaction (1.1) and compare them both with those obtained from the approximations given in ref. [9] as well as the exact results in ref [3]. Details and long formulae will be presented in appendices A, B and C.

2. Radiative corrections to the quark–antiquark reaction

The momentum assignment of the lowest order process as given in (1 2) will be denoted by

$$\mathrm{q}(k_1) + \bar{\mathrm{q}}(k_2) \to \mathrm{Q}(p_1) + \overline{\mathrm{Q}}(p_2) \tag{2.1}$$

Unless stated otherwise we assume the heavy antiquark to be detected The graph which contributes to the Born amplitude is shown in fig 1. For the kinematical variables we choose

$$s = 2k_1\cdot k_2, \qquad t_1 = t - m^2 = (k_2 - p_2)^2 - m^2,$$

$$u_1 = u - m^2 = (k_1 - p_2)^2 - m^2. \tag{2.2}$$

Fig. 1. The lowest order Feynman diagram contributing to the amplitude for the reaction $\mathrm{q}(k_1) + \bar{\mathrm{q}}(k_2) \to \mathrm{Q}(p_1) + \overline{\mathrm{Q}}(p_2)$. The arrows denote the flow of charge of the quarks. The thicker lines are those of the heavy quarks.

Since the cross sections for the Born process and its radiative corrections have to be evaluated in n-dimensions the algebra was performed by using the program FORM* The square of the Born amplitude summed over the initial and final spins can be written as

$$\sum M^{\mathrm{B}} M^{\mathrm{B}*} = 4g^4 N C_{\mathrm{F}} A_{\mathrm{QED}}, \tag{2.3}$$

where N refers to the gauge group SU(N), $C_{\mathrm{F}} = (N^2 - 1)/2N$ is the colour factor corresponding to the fundamental representation of the quarks and A_{QED} stands for the QED analogue of the process in (2 1). It is given by

$$A_{\mathrm{QED}} = \frac{t_1^2 + u_1^2}{s^2} + \frac{2m^2}{s} + \frac{\epsilon}{2}, \tag{2.4}$$

with $\epsilon = n - 4$ Notice that like in the gluon–gluon fusion process (see ref. [4]) the ϵ terms are mass independent Averaging over the initial quark/antiquark spins and colours we find that the result for the Born cross section in n-dimensions can be expressed as follows [4]

$$s^2 \frac{\mathrm{d}^2\sigma^{(0)}_{q\bar{q}}}{\mathrm{d}t_1\,\mathrm{d}u_1} = \tfrac{1}{4} K_{q\bar{q}} \frac{\pi S_\epsilon}{\Gamma(1+\epsilon/2)} \left(\frac{t_1 u_1 - s m^2}{\mu^2 s} \right)^{\epsilon/2} \delta(s + t_1 + u_1) \sum M^{\mathrm{B}} M^{\mathrm{B}*}, \tag{2.5}$$

where $K_{q\bar{q}} = N^{-2}$ is the colour average factor for two quarks in the initial state The mass parameter μ in eq. (2.5) originates from the dimensionality of the gauge coupling constant g in n-dimensions. The constant $S_\epsilon = (4\pi)^{-2-\epsilon/2}$ originates from the n-dimensional integration over the solid angle and the remaining factor comes from the two-particle phase space integral.

The virtual corrections to the differential cross section in eq (2.5) require the calculation of the Feynman diagrams shown in fig 2 The ultraviolet (UV), infrared (IR) and the collinear or mass (M) singularities which appear in the graphs are regularized by n-dimensional regularization In order to distinguish the quarks which show up in the internal fermion loop from the produced heavy flavours, we indicate the first ones by the mass m_f. For the internal gluon propagator we have chosen the Feynman gauge. The computation of the virtual amplitude M^{V} has been done as follows For the Lorentz algebra we used the program FORM*. The Feynman integrals which contain loop momenta in the

* The symbolic manipulation program FORM was written by J A M Vermaseren at NIKHEF-H Version 1 0 of this program and its manual are available from the author

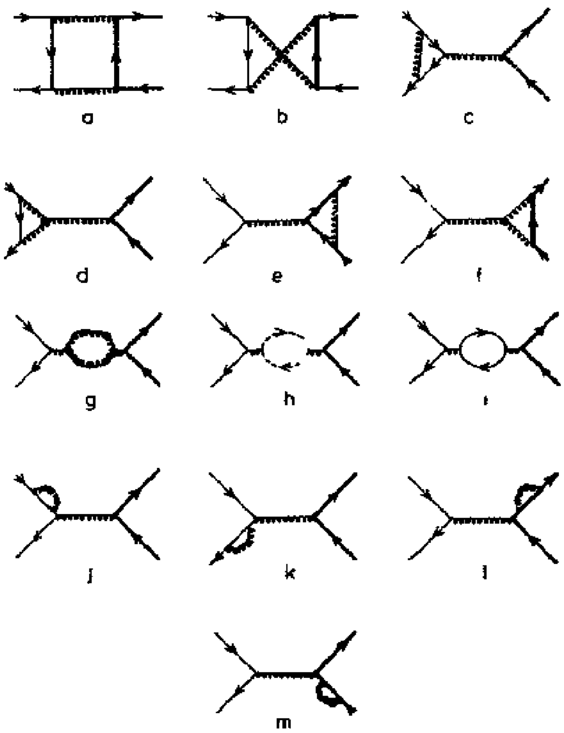

Fig 2 The order α_s^3 Feynman diagrams for the virtual corrections to the reaction $q(k_1)+\bar{q}(k_2) \to Q(p_1)+\bar{Q}(p_2)$

numerator have been dealt with using an adapted version of the reduction program of Passarino and Veltman [16]. This program has been extended (see ref [17]) to account for the IR and M singularities. In this way we could reduce all the Feynman integrals to a set of elementary integrals which are listed in appendix A of ref [4] The virtual cross section is obtained from the interference term between the virtual and the Born amplitude Summing over the initial and final quark/antiquark spins this terms will be denoted by

$$\sum (M^{V}M^{B*}+M^{B}M^{V*}) = g^{6}\left[NC_F^2 V_F + NC_A C_F V_A + NC_F V_f\right], \qquad (2\,6)$$

where $C_A = N$ is the colour factor corresponding to the adjoint representation of the gluon The three contributions to the interference term, i.e. V_F, V_A and V_f, stand for the abelian (QED), the non-abelian and the fermion loop parts respectively In the last contribution the sum over all flavours is implicitly understood The expressions for V_F and V_A are so lengthy that they will not be given here. However they can be easily reconstructed from the reduced virtual plus soft cross section which is obtained after performing renormalization and mass factorization The expression for V_f can be derived from (2.11) and (2 12) below

The virtual unrenormalized cross section becomes

$$\left(s^2 \frac{d^2\sigma^{(1)}_{q\bar{q}}}{dt_1\, du_1}\right)^{V} = \tfrac{1}{4} K_{q\bar{q}} \frac{\pi S_\epsilon}{\Gamma(1+\epsilon/2)} \left(\frac{t_1 u_1 - s m^2}{\mu^2 s}\right)^{\epsilon/2}$$

$$\times \delta(s + t_1 + u_1) \sum \left(M^{V} M^{B*} + M^{B} M^{V*}\right), \qquad (2.7)$$

where $K_{q\bar{q}}$ is defined below (2.5) Using the same shorthand notation as in eq. (2.6) we can split the virtual cross section as follows

$$\left(d\sigma^{(1)}_{q\bar{q}}\right)^{V} = \left(d\sigma^{(1)}_{q\bar{q}\,F}\right)^{V} + \left(d\sigma^{(1)}_{q\bar{q}\,A}\right)^{V} + \left(d\sigma^{(1)}_{q\bar{q}\,f}\right)^{V}. \qquad (2.8)$$

In the explicit expression for the virtual cross section we observe single and double pole terms of the type ϵ^{-i} $(i = 1,2)$ which are due to UV, IR and M singularities. Double pole terms only appear when IR and M singularities coincide The latter show up in the F part of the virtual cross section only Moreover this part contains all the M singularities and has no UV divergences related to coupling constant renormalization. These divergences can only be attributed to the A and f part. UV divergences related to mass renormalization appear at the external fermion legs of the Feynman graphs contributing to the F and A part These two parts also contain all IR divergences. The UV divergences are removed by renormalization Since the cross section is a renormalization group invariant we can limit ourselves to mass and coupling constant renormalization. Starting with mass renormalization we choose the on-shell renormalization scheme This can be achieved by replacing the bare mass in the Born cross section by the renormalized mass

$$m_b \to m\left\{1 + \frac{g^2}{16\pi^2} C_F \left(\frac{6}{\epsilon} + 3\gamma_E - 3\ln 4\pi - 4 - 3\ln\frac{\mu^2}{m^2}\right)\right\}. \qquad (2.9)$$

For the coupling constant renormalization we allow ourselves more freedom as long as we limit ourselves to gauge invariant subtraction schemes. In the first instance we choose the $\overline{\mathrm{MS}}$ scheme which can be achieved by replacing the bare coupling constant in the Born cross section by the renormalized one

$$g_b \to g(\mu_R^2)\left\{1 + \frac{\alpha_S(\mu_R^2)}{8\pi}\left(\frac{2}{\epsilon} + \gamma_E - \ln 4\pi + \ln\frac{\mu_R^2}{\mu^2}\right)\beta_0\right\}, \qquad (2.10)$$

with $\beta_0 = 11N/3 - 2n_f/3$ where n_f is the number of flavours in the internal fermion loop. Furthermore we have used $g^2(\mu_R^2) \equiv 4\pi\alpha_S(\mu_R^2)$, where μ_R^2 stands for the coupling constant renormalization scale. The renormalized virtual cross section is now given by

$$\left(s^2\frac{\mathrm{d}^2\sigma_{q\bar{q}}^{(1)}}{\mathrm{d}t_1\,\mathrm{d}u_1}\right)_{\mathrm{R}}^{\mathrm{V}} = \left(s^2\frac{\mathrm{d}^2\sigma_{q\bar{q}}^{(1)}}{\mathrm{d}t_1\,\mathrm{d}u_1}\right)^{\mathrm{V}} + \frac{\alpha_s(\mu_{\mathrm{R}}^2)}{2\pi}\left(\frac{2}{\epsilon} + \gamma_{\mathrm{E}} - \ln 4\pi + \ln\frac{\mu_{\mathrm{R}}^2}{\mu^2}\right)\beta_0\left(s^2\frac{\mathrm{d}^2\sigma_{q\bar{q}}^{(0)}}{\mathrm{d}t_1\,\mathrm{d}u_1}\right), \tag{2.11}$$

where mass renormalization in the first term of the r.h.s. of the above equation is already implicitly understood. The fermion loop contribution to the renormalized virtual cross section in (2.11) for $s \geqslant 4m_{\mathrm{f}}^2$ is given by

$$\left(s^2\frac{\mathrm{d}^2\sigma_{q\bar{q},\mathrm{f}}^{(1)}}{\mathrm{d}t_1\,\mathrm{d}u_1}\right)_{\mathrm{R}}^{\mathrm{V}} = \frac{\alpha_s(\mu_{\mathrm{R}}^2)}{3\pi}\sum_{\mathrm{f}=\mathrm{L,H}}\left[\ln\frac{m_{\mathrm{f}}^2}{\mu_{\mathrm{R}}^2} - \frac{5}{3} - \frac{4m_{\mathrm{f}}^2}{s} - \sqrt{1-\frac{4m_{\mathrm{f}}^2}{s}}\left(1+\frac{2m_{\mathrm{f}}^2}{s}\right)\ln x_{\mathrm{f}}\right]s^2\frac{\mathrm{d}^2\sigma_{q\bar{q}}^{(0)}}{\mathrm{d}t_1\,\mathrm{d}u_1}, \tag{2.12}$$

where the summation is taken over the light (L) and heavy (H) quark contributions and

$$x_{\mathrm{f}} = \frac{1-\sqrt{1-4m_{\mathrm{f}}^2/s}}{1+\sqrt{1-4m_{\mathrm{f}}^2/s}}. \tag{2.13}$$

In the case that $s < 4m_{\mathrm{f}}^2$ we have the replacement

$$\sqrt{1-\frac{4m_{\mathrm{f}}^2}{s}}\ln x_{\mathrm{f}} \to -2\sqrt{\frac{4m_{\mathrm{f}}^2}{s}-1}\,\arctan\left(\frac{1}{\sqrt{4m_{\mathrm{f}}^2/s-1}}\right). \tag{2.14}$$

Besides the usual $\overline{\mathrm{MS}}$ scheme we can choose another one [2,3]. This scheme is given by the prescription that in the limit of small momenta the heavy quarks in the fermion loop are decoupled. This can be achieved by subtracting the heavy fermion loop at zero external momenta. In this case we get

$$\left(s^2\frac{\mathrm{d}^2\sigma_{q\bar{q},\mathrm{f}}^{(1)}}{\mathrm{d}t_1\,\mathrm{d}u_1}\right)_{\mathrm{R}}^{\mathrm{V}} = \frac{\alpha_s(\mu_{\mathrm{R}}^2)}{3\pi}\left[\sum_{\mathrm{f}=\mathrm{L,H}}\left\{-\frac{5}{3} - \frac{4m_{\mathrm{f}}^2}{s} - \sqrt{1-\frac{4m_{\mathrm{f}}^2}{s}}\left(1+\frac{2m_{\mathrm{f}}^2}{s}\right)\ln x_{\mathrm{f}}\right\} + \sum_{\mathrm{f}=\mathrm{L}}\ln\frac{m_{\mathrm{f}}^2}{\mu_{\mathrm{R}}^2}\right]s^2\frac{\mathrm{d}^2\sigma_{q\bar{q}}^{(0)}}{\mathrm{d}t_1\,\mathrm{d}u_1}. \tag{2.15}$$

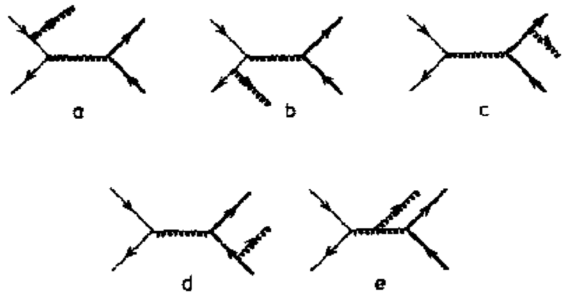

Fig 3 The order g^3 Feynman diagrams contributing to the amplitude for the gluon bremsstrahlung process $q(k_1)+\bar{q}(k_2)\to g(k_3)+Q(p_1)+\bar{Q}(p_2)$ The graphs for the processes $g(k_1)+\bar{q}(k_2)\to\bar{q}(k_3)+Q(p_1)+\bar{Q}(p_2)$ and $g(k_1)+q(k_2)\to q(k_3)+Q(p_1)+\bar{Q}(p_2)$ can be obtained via crossing

Notice that the limit $m_l \to 0$ in the sum over the light flavours is well defined The latter renormalization scheme implies that the heavy flavours do not contribute to the evolution of the running coupling constant From now on we will suppress the scale dependence of the coupling constant and refer to it as g or α_S instead of $g(\mu_R^2)$ or $\alpha_S(\mu_R^2)$

Next we have to calculate the real gluon bremsstrahlung corrections to the lowest order process (1 2) The gluon bremsstrahlung cross section is given by the following process

$$q(k_1)+\bar{q}(k_2)\to g(k_3)+Q(p_1)+\bar{Q}(p_2) \tag{2 16}$$

The five Feynman diagrams which contribute to the amplitude M^R are shown in fig 3. In the calculation of these diagrams we introduced the following ten kinematical invariants [4]

$$\begin{aligned}
s &= (k_1+k_2)^2, & u_1 &= (k_1-p_2)^2-m^2 = u-m^2,\\
s_3 &= (k_3+p_2)^2-m^2, & t' &= (k_2-k_3)^2,\\
s_4 &= (k_3+p_1)^2-m^2, & u' &= (k_1-k_3)^2,\\
s_5 &= (p_1+p_2)^2 = -u_5, & u_6 &= (k_2-p_1)^2-m^2,\\
t_1 &= (k_2-p_2)^2-m^2 = t-m^2, & u_7 &= (k_1-p_1)^2-m^2,
\end{aligned} \tag{2.17}$$

where $k_1+k_2=k_3+p_1+p_2$. The invariants s, t_1 and u_1 were already used in the calculation of the Born graphs (2.2) and the virtual graphs. Since we are considering a two-to-three body process only five of the invariants are linearly independent. The square of the amplitude was calculated in n dimensions up to order ϵ^2 ($\epsilon = n-4$) in order to account for the IR and M singularities which show up in the real gluon cross section. We checked algebraically that the $n=4$ part of the square of the matrix element agrees with the expression found in ref [18] The square of the amplitude will be denoted by

$$\sum M^{\mathrm{R}} M^{\mathrm{R}*} = g^6\left[NC_{\mathrm{F}}^2 R_{\mathrm{F}} + NC_{\mathrm{A}} C_{\mathrm{F}} R_{\mathrm{A}}\right] \tag{2.18}$$

Here the summation over initial and final spins/polarizations is implicitly understood. The colour factors C_{F} and C_{A} were already defined in (2.3) and (2.6). Averaging over the initial spins and colours the cross section can be written in the following form (see appendix B in ref [4]),

$$\left(s^2 \frac{\mathrm{d}^2\sigma_{q\bar{q}}^{(1)}}{\mathrm{d}t_1\,\mathrm{d}u_1}\right)^{\mathrm{R}} = \tfrac{1}{8} K_{q\bar{q}} \frac{S_\epsilon^2 \mu^{-\epsilon}}{\Gamma(1+\epsilon)} \left(\frac{t_1 u_1 - s m^2}{\mu^2 s}\right)^{\epsilon/2} \frac{s_4^{1+\epsilon}}{(s_4+m^2)^{1+\epsilon/2}} \int \mathrm{d}\Omega_n \sum M^{\mathrm{R}} M^{\mathrm{R}*}, \tag{2.19}$$

with $s_4 = s + t_1 + u_1$ and $\mathrm{d}\Omega_n = \sin^{1+\epsilon}\theta_1\,\mathrm{d}\theta_1 \sin^{\epsilon}\theta_2\,\mathrm{d}\theta_2$ Analogous to the virtual cross section we can decompose (2.19) into

$$\left(\mathrm{d}\sigma_{q\bar{q}}^{(1)}\right)^{\mathrm{R}} = \left(\mathrm{d}\sigma_{q\bar{q}\,\mathrm{F}}^{(1)}\right)^{\mathrm{R}} + \left(\mathrm{d}\sigma_{q\bar{q}\,\mathrm{A}}^{(1)}\right)^{\mathrm{R}}. \tag{2.20}$$

In order to compute the real gluon cross section we follow the procedure as outlined in refs. [4, 19]. To this purpose we split the cross section into a hard gluon ($s_4 > \Delta$) and a soft gluon ($s_4 < \Delta$) part. The parameter Δ is chosen in such a way that it can be neglected with respect to mass terms like m^2 and the kinematical invariants s, t_1 and u_1. Starting with the hard gluon correction we can neglect the terms in the matrix element squared which are proportional to ϵ^2. This is because the hard collinear divergences only provide us with single pole terms $1/\epsilon$ In order to perform the angular integrations the expression for $\Sigma M^{\mathrm{R}} M^{\mathrm{R}*}$ has to be partially fractioned so that the whole angular dependence can be attributed to only two factors containing the angular terms. This procedure is extensively described in sect. 4 and appendix C of ref. [4]. The hard gluon–parton cross sections become

$$\begin{aligned}
\left(s^2 \frac{\mathrm{d}^2\sigma_{q\bar{q}\,\mathrm{F}}^{(1)}}{\mathrm{d}t_1\,\mathrm{d}u_1}\right)^{\mathrm{H}} = {} & \tfrac{1}{4}\alpha_s^3 K_{q\bar{q}} N C_{\mathrm{F}}^2 \frac{1}{(4\pi)^{\epsilon/2}} \frac{1}{\Gamma(1+\epsilon/2)} \left(\frac{t_1 u_1 - s m^2}{\mu^2 s}\right)^{\epsilon/2} \\
& \times \left[\left[\left\{\frac{2}{\epsilon} + \gamma_E - \ln 4\pi + \ln \frac{s_4^2}{\mu^2 (s_4 + m^2)}\right\}\right.\right. \\
& \times \left\{-\frac{1}{u_1}\left(\frac{u_1^2 + (s+t_1)^2}{s_4(s+t_1)}\right)\left(\frac{t_1^2 + (s+t_1)^2}{s^2} - \frac{2m^2(s+t_1)}{s u_1} + \frac{\epsilon}{2}\right)\right\} \\
& \left. - \frac{s_4}{u_1(s+t_1)}\left\{\frac{t_1^2 + (s+t_1)^2}{s^2} - \frac{2m^2 [illegible] t_1}{u_1 s}\right\}\right] + (t_1 \leftrightarrow u_1)\Bigg] \\
& + \left(\tfrac{1}{4}\right)^{[illegible]} \frac{\alpha_s^3}{\pi} K_{q\bar{q}} N C_{\mathrm{F}}^2 \frac{s_4}{s_4 + m^2} \left(\int \mathrm{d}\Omega_n R_{\mathrm{F}}\right)^{\text{finite}},
\end{aligned} \tag{2.21}$$

and

$$\left(s^2\frac{d^2\sigma^{(1)}_{q\bar{q},A}}{dt_1\,du_1}\right)^{H} = \left(\frac{1}{2}\right)^5 \frac{\alpha_S^3}{\pi} K_{q\bar{q}} N C_A C_F \frac{s_4}{s_4+m^2}\left(\int d\Omega_4\, R_A\right) \qquad (2.22)$$

The amplitudes squared R_F and R_A can be obtained from expression (10) in ref [18] The pole terms originating from t'^{-1} and u'^{-1} which appear in the ϵ^i ($i = 0, 1$) parts of the matrix element are presented between the curly brackets of expression (2.21) Notice that $(d\sigma^{(1)}_{q\bar{q},A})^{H}$ does not have collinear divergences This feature has also been observed for $(d\sigma^{(1)}_{q\bar{q},A})^{V}$ [see eq. (2.8)]

Finally we have to calculate the soft gluon cross section The soft gluon amplitude can be obtained from the matrix element in (2.18) by applying the eikonal approximation. In the limit when the gluon momentum k_3 in (2.16) gets soft the kinematical invariants in the two-to-three body process become

$$\begin{aligned} &s_3 \to 0, \qquad s_4 \to 0, \qquad t' \to 0, \qquad u' \to 0, \\ &u_5 \to -s, \qquad u_6 \to u_1, \qquad u_7 \to t_1, \end{aligned} \qquad (2.23)$$

while the other invariants remain unaltered. The soft matrix element M^S can be written in the same form as in (2.18)

$$\sum M^S M^{S*} = g^6\left[N C_F^2 S_F + N C_A C_F S_A\right], \qquad (2.24)$$

with

$$S_F = 16\left[\frac{s}{t'u'} + \frac{2t_1}{t's_3} + \frac{2t_1}{u's_4} - \frac{2u_1}{t's_4} - \frac{2u_1}{u's_3} + \frac{(s-2m^2)}{s_3 s_4} - \frac{m^2}{s_3^2} - \frac{m^2}{s_4^2}\right]A_{QED}, \qquad (2.25)$$

and

$$S_A = 8\left[-\frac{s}{t'u'} - \frac{t_1}{t's_3} - \frac{t_1}{u's_4} + \frac{2u_1}{t's_4} + \frac{2u_1}{u's_3} - \frac{s-2m^2}{s_3 s_4}\right]A_{QED}. \qquad (2.26)$$

The soft gluon cross section is obtained from the expression

$$\left(s^2\frac{d^2\sigma^{(1)}_{q\bar{q}}}{dt_1\,du_1}\right)^{S} = \tfrac{1}{8}K_{q\bar{q}}\frac{S_\epsilon^2\mu^{-\epsilon}}{\Gamma(1+\epsilon)}\left(\frac{t_1u_1 - sm^2}{\mu^2 s}\right)^{\epsilon/2}\delta(s+t_1+u_1)$$
$$\times\int_0^{\Delta} ds_4 \frac{s_4^{1+\epsilon}}{(s_4+m^2)^{1+\epsilon/2}}\int d\Omega_n \sum M^S M^{S*}. \qquad (2.27)$$

Performing the integrals over the angles and the invariant s_4 we get

$$\begin{aligned}\left(s^2\frac{\mathrm{d}^2\sigma^{(1)}_{q\bar{q},F}}{\mathrm{d}t_1\,\mathrm{d}u_1}\right)^S &= K_{q\bar{q}}NC_F^2F(s,t_1,u_1)\delta(s+t_1+u_1)\\
&\quad\times\Bigg[\frac{16}{\epsilon^2}+\frac{8}{\epsilon}\ln\frac{sm^2}{t_1u_1}+2\ln^2\frac{sm^2}{t_1u_1}+4\,\mathrm{Li}_2\left(1-\frac{sm^2}{t_1u_1}\right)+\frac{4(s-2m^2)}{\sqrt{s^2-4sm^2}}\\
&\qquad\times\left\{-\frac{2}{\epsilon}\ln x-\ln x+2\,\mathrm{Li}_2(x)+2\,\mathrm{Li}_2(-x)-\ln^2x\right.\\
&\qquad\qquad\left.+2\ln x\ln(1-x^2)-\zeta(2)\right\}\\
&\qquad-\frac{8}{\epsilon}+4+\frac{32}{\epsilon}\ln\frac{t_1}{u_1}-16\ln x\ln\frac{t_1}{u_1}\\
&\qquad-16\,\mathrm{Li}_2\left(1-\frac{u_1}{xt_1}\right)+16\,\mathrm{Li}_2\left(1-\frac{t_1}{xu_1}\right)-6\zeta(2)\Bigg], \qquad (2.28)\end{aligned}$$

$$\begin{aligned}\left(s^2\frac{\mathrm{d}^2\sigma^{(1)}_{q\bar{q},A}}{\mathrm{d}t_1\,\mathrm{d}u_1}\right)^S &= K_{q\bar{q}}NC_AC_FF(s,t_1,u_1)\delta(s+t_1+u_1)\\
&\quad\times\Bigg[-\frac{4}{\epsilon}\ln\frac{sm^2}{t_1u_1}-\ln^2\frac{sm^2}{t_1u_1}-2\,\mathrm{Li}_2\left(1-\frac{sm^2}{t_1u_1}\right)-\frac{2(s-2m^2)}{\sqrt{s^2-4sm^2}}\\
&\quad\times\left\{-\frac{2}{\epsilon}\ln x+2\,\mathrm{Li}_2(x)+2\,\mathrm{Li}_2(-x)-\ln^2x+2\ln x\ln(1-x^2)-\zeta(2)\right\}\\
&\quad+\frac{12}{\epsilon}\ln\frac{u_1}{t_1}+6\ln x\ln\frac{t_1}{u_1}-\ln^2x+\ln^2\frac{t_1}{u_1}\\
&\qquad-6\,\mathrm{Li}_2\left(1-\frac{t_1}{xu_1}\right)+6\,\mathrm{Li}_2\left(1-\frac{u_1}{xt_1}\right)\Bigg], \qquad (2.29)\end{aligned}$$

with

$$x=\frac{1-\sqrt{1-4m^2/s}}{1+\sqrt{1-4m^2/s}}, \qquad 0\leqslant x\leqslant 1, \qquad (2.30)$$

and the common factor F defined by

$$F(s,t_1,u_1)=\frac{1}{16\pi}g^6\frac{S_\epsilon}{\Gamma(1+\epsilon/2)}$$

$$\times\exp\left(\frac{\epsilon}{2}(\gamma_{\mathrm{E}}-\ln 4\pi)\right)\left(\frac{t_1u_1-sm^2}{\mu^2 s}\right)^{\epsilon/2}\left(\frac{\Delta^2}{\mu^2m^2}\right)^{\epsilon/2}A_{\mathrm{QED}} \quad (2.31)$$

In the above expressions $\zeta(2)=\pi^2/6$ and γ_{E} is the Euler constant $\mathrm{Li}_2(x)$ is the dilogarithmic function as defined in ref. [20] Note that all differential cross sections are proportional to the Born cross section This is in contrast with what we observed in the gluon–gluon fusion process (1.3) (see ref. [4]). Addition of the renormalized virtual contribution (2.11) and the soft contribution (2.27) leads to the cancellation of the IR singularities present in both of them The left-over collinear divergences from the initial state gluon radiation are responsible for the single pole terms. The latter can be removed by mass factorization as will be shown in sect. 4. Finally we want to comment on the cross sections calculated above All expressions except for the fermion loop contribution in eq. (2.15) are asymmetric under interchanging t_1 and u_1. This is in contrast with our findings for the gluon–gluon fusion process which is symmetric in t_1 and u_1. In the case of the virtual cross section this asymmetry can be traced back to the interference between the Born and the box graphs In the real gluon cross section it can be attributed to the interferences between initial and final state gluons. In the abelian (QED) part of the above process this phenomenon is known as forward–backward asymmetry or charge asymmetry. It is caused by interference between $C=+$ and $C=-$ states, where C denotes charge conjugation.

Notice that the above cross sections have been presented for the case that only the heavy antiquark is detected. Here the variables t_1 and u_1 denote the square of the four-momentum transfer of the detected heavy antiquark with respect to the incoming light antiquark and quark respectively [see eq. (2.17)]. The cross sections in the case that the heavy quark is detected can be derived in an analogous way The expressions are related to those obtained for the heavy antiquark as will be shown in sect 4

3. The (anti)quark–gluon subprocess

The matrix element $M_{g\bar{q}}$ of the antiquark–gluon process

$$g(k_1)+\bar{q}(k_2)\rightarrow\bar{q}(k_3)+Q(p_1)+\bar{Q}(p_2), \quad (3.1)$$

can be obtained from the amplitude calculated for the quark–antiquark reaction

(2.16), i.e. M^{R} via crossing. The latter can be achieved by multiplying $\sum M_{\mathrm{R}} M_{\mathrm{R}}^*$ with an overall minus sign and interchanging $k_1 \leftrightarrow -k_3$. This implies that the invariants listed in eq. (2.17) which appear in the squared amplitude $\sum M_{g\bar{q}} M_{g\bar{q}}^*$ are obtained from those present in $\sum M_{\mathrm{R}} M_{\mathrm{R}}^*$ in eq. (2.18) via the following replacements

$$s \leftrightarrow t', \qquad s_3 \leftrightarrow u_1, \qquad s_4 \leftrightarrow u_7, \tag{3.2}$$

whereas the other invariants remain unchanged. The expression for $\sum M_{g\bar{q}} M_{g\bar{q}}^*$ can again be decomposed in its colour parts like in eq. (2.18):

$$\sum M_{g\bar{q}} M_{g\bar{q}}^* = g^6 \left[N C_{\mathrm{F}}^2 R_{g\bar{q},\mathrm{F}} + N C_{\mathrm{A}} C_{\mathrm{F}} R_{g\bar{q},\mathrm{A}} \right], \tag{3.3}$$

where one has summed over all initial and final spins and/or polarizations. In computing the differential cross section one has to bear in mind that in n dimensions the gluon has $n-2$ degrees of freedom. This one has to implement in the cross section when one averages over the initial gluon polarization. Therefore for each gluon in the initial state one gets a factor $(n-2)^{-1}$ instead of $1/2$. This is very important if we have to deal with non-diagonal processes in which the parton splitting functions (see sect. 4) are non-diagonal. In this case the reduced cross sections have either one gluon more or one gluon less than the original parton process. When the number of gluons in the initial state of the cross sections mentioned above are the same then one can extract an identical overall factor. Hence it does not matter if one takes the limit $n \to 4$ before or after the mass factorization. An example is the gluon-gluon fusion reaction (1.3) where $\mathrm{d}\sigma_{gg}^{(1)}$ and $\mathrm{d}\sigma_{gg}^{(0)}$ have the same numbers of gluons (here two) in the initial state. The antiquark-gluon differential cross section is therefore given by

$$s^2 \frac{\mathrm{d}^2 \sigma_{g\bar{q}}^{(1)}}{\mathrm{d}t_1\, \mathrm{d}u_1} = \tfrac{1}{4} K_{gq} \frac{S_\varepsilon^{-1} \mu^{-\varepsilon}}{(1+\varepsilon/2)\Gamma(1+\varepsilon)} \left(\frac{t_1 u_1 - s m^2}{\mu^2 s} \right)^{\varepsilon/2}$$

$$\times \frac{s_4^{1+\varepsilon}}{(s_4 + m^2)^{1+\varepsilon/2}} \int \mathrm{d}\Omega_n \sum M_{g\bar{q}} M_{g\bar{q}}^*, \tag{3.4}$$

with $K_{gq} = (N(N^2-1))^{-1}$ and the $(1+\varepsilon/2)^{-1}$ originates from the averaging over the initial gluon polarization. Since there are no gluons in the final state one encounters collinear divergences only. Therefore, we only have to include the ε part of the matrix element squared. The partial fractioning proceeds in the same way as in sect. 2 (see ref. [4]). According to expression (3.3) we find the following cross sections.

$$
\begin{aligned}
\left(s^2\frac{\mathrm{d}^2\sigma^{(1)}_{g\bar{q},F}}{\mathrm{d}t_1\,\mathrm{d}u_1}\right) = {}& \tfrac{1}{2}\alpha_S^3 K_{gq} N C_F^2 \frac{1}{(4\pi)^{\epsilon/2}}\,\frac{1}{\Gamma(1+\epsilon/2)}\left(\frac{t_1u_1-sm^2}{\mu^2 s}\right)^{\epsilon/2} \\
& \times\Bigg[\left\{\frac{2}{\epsilon}+\gamma_E-\ln 4\pi+\ln\frac{s_4^2}{\mu^2(s_4+m^2)}\right\} \\
& \quad\times\left\{\frac{s+t_1}{u_1^2}\left(\frac{s_4^2+(s+t_1)^2}{(s+t_1)^2}\right)\left(\frac{t_1^2+(s+t_1)^2}{-t_1(s+t_1)}+\frac{4m^2s}{t_1u_1}\left(1-\frac{m^2s}{t_1u_1}\right)\right)\right. \\
& \qquad\left.-\frac{1}{t_1}\,\frac{s_4^2+t_1^2}{(s+u_1)^2}\left(\frac{(s+u_1)^2+u_1^2}{s^2}-\frac{2m^2(s+u_1)}{st_1}\right)\right\} \\
& \quad-\frac{s+t_1}{u_1^2}\left(\frac{s_4^2+(s+t_1)^2}{(s+t_1)^2}\right)\left(-2+\frac{4m^2s}{t_1u_1}\left(1-\frac{m^2s}{t_1u_1}\right)\right) \\
& \quad-\frac{t_1^2+(s+t_1)^2}{t_1(s+t_1)^2}-\frac{s_4^2+t_1^2}{t_1(s+u_1)^2} \\
& \quad+\frac{2s_4}{(s+u_1)^2}\left(\frac{(s+u_1)^2+u_1^2}{s^2}-\frac{2m^2(s+u_1)}{st_1}\right)\Bigg] \\
& +\left(\frac{1}{2}\right)^5\frac{\alpha_S^3}{\pi}K_{gq}NC_F^2\frac{s_4}{s_4+m^2}\left(\int \mathrm{d}\Omega_n\, R_{gq,F}\right)^{\text{finite}}, \qquad (3.5)
\end{aligned}
$$

and

$$
\begin{aligned}
\left(\text{[illegible]}\right) = {}& \text{[illegible]}\,K_{gq}NC_AC_F\frac{1}{(4\pi)^{\epsilon/2}}\,\frac{1}{\Gamma(1+\epsilon/2)}\left(\frac{t_1u_1-sm^2}{\mu^2 s}\right)^{\epsilon/2} \\
& \times\Bigg[\left\{\frac{2}{\epsilon}+\gamma_E-\ln 4\pi+\ln\frac{s_4^2}{\mu^2(s_4+m^2)}\right\} \\
& \quad\times\left\{\frac{t_1(s+t_1)^2}{s^2u_1^2}\left(\frac{s_4^2+(s+t_1)^2}{(s+t_1)^2}\right)\left(\frac{t_1^2+(s+t_1)^2}{-t_1(s+t_1)}+\frac{4m^2s}{t_1u_1}\left(1-\frac{m^2s}{t_1u_1}\right)\right)\right\} \\
& -\frac{t_1(s+t_1)^2}{s^2u_1^2}\left(\frac{s_4^2+(s+t_1)^2}{(s+t_1)^2}\right)\left(-2+\frac{4m^2s}{t_1u_1}\left(1-\frac{m^2s}{t_1u_1}\right)\right)-\frac{t_1^2+(s+t_1)^2}{s^2(s+t_1)}\Bigg] \\
& +\left(\frac{1}{2}\right)^5\frac{\alpha_S^3}{\pi}K_{gq}NC_AC_F\frac{s_4}{s_4+m^2}\left(\int \mathrm{d}\Omega_n\, R_{gq,A}\right)^{\text{finite}}. \qquad (3.6)
\end{aligned}
$$

Notice that $d\sigma^{(1)}_{g\bar{q},\Gamma}$ contains pole terms of the type t'^{-1} as well as u'^{-1} whereas in $d\sigma^{(1)}_{g\bar{q},A}$ only poles of the type t'^{-1} appear. Like in the quark–antiquark subprocess the above cross sections are not symmetric under $t_1 \leftrightarrow u_1$. Note that in the above expressions the variables t_1 and u_1 are the square of the four-momentum transfer of the heavy antiquark with respect to the light antiquark and gluon respectively. If the light antiquark in the initial state is replaced by the light quark the above expressions will change. However we will show explicitly in sect. 4 that $d\sigma_{gq}(t_1,u_1)$ and $d\sigma_{g\bar{q}}(t_1,u_1)$ are related to each other. A similar relation holds if the heavy antiquark in the final state is replaced by the heavy quark.

4. Mass factorization

The various parton cross sections which have been computed in the previous sections still contain initial state collinear (M) divergences. These singularities have to be removed via mass factorization. The collinear-singular parton cross section $d\sigma_{ij}$ can be written to all orders in α_s as

$$s^2\frac{d^2\sigma_{ij}(s,t_1,u_1,\mu^2,\epsilon)}{dt_1\,du_1} = \int_0^1\frac{dx_1}{x_1}\int_0^1\frac{dx_2}{x_2}\Gamma_{li}(x_1,Q^2,\mu^2,\epsilon)\Gamma_{mj}(x_2,Q^2,\mu^2,\epsilon)$$

$$\times\hat{s}^2\frac{d^2\hat{\sigma}_{lm}(\hat{s},\hat{t}_1,\hat{u}_1,Q^2)}{d\hat{t}_1\,d\hat{u}_1}, \qquad (4.1)$$

where $\hat{s}=x_1x_2s$, $\hat{t}_1=x_1t_1$, $\hat{u}_1=x_2u_1$. The Γ_{ij} are the splitting functions which have been calculated up to order α_s^2 and can be found in the literature [21]. They contain the collinear singularities indicated by ϵ and further depend on the mass factorization scale Q^2, which is of the order of s, t_1, u_1. The parameter μ^2 is an artefact of n-dimensional regularization because in this method the gauge coupling constant g gets a dimension. The reduced cross sections $d\hat{\sigma}_{lm}$ have no collinear divergences and are therefore finite in the limit $\epsilon \to 0$. They further depend on the factorization scale Q^2 and the variables $\hat{s},\hat{t}_1,\hat{u}_1$. For convenience we have set the factorization scale equal to the renormalization scale μ_R^2 in eq. (4.1). Like the Γ_{ij} the parton cross sections $d\sigma_{ij}$ and $d\hat{\sigma}_{lm}$ can be expanded in a power series in α_s. Up to first order in α_s, Γ_{ij} takes the following form

$$\Gamma_{ij}(x,Q^2,\mu^2,\epsilon) = \delta_{ij}\delta(1-x) + \frac{\alpha_s}{2\pi}\left[P_{ij}(x)\frac{2}{\epsilon} + f_{ij}(x,Q^2,\mu^2)\right], \qquad (4.2)$$

where P_{ij} denotes the Altarelli–Parisi splitting functions [22]. The functions f_{ij} depend on the chosen mass factorization scheme. In this article we will compute the reduced parton cross sections in two different schemes, i.e. $\overline{\text{MS}}$ and DIS. In $\overline{\text{MS}}$

the function f_{ij} gets the form

$$f_{ij}^{\overline{\rm MS}}(x,Q^2,\mu^2) = P_{ij}(x)\left(\gamma_{\rm E} - \ln 4\pi + \ln\frac{Q^2}{\mu^2}\right), \tag{4.3}$$

whereas in DIS f_{ij} is determined by the parton cross section in the corresponding deep inelastic lepton–hadron scattering process. Starting with the quark–antiquark annihilation process we get the following expressions

$$P_{\rm q\bar q}(x) = C_{\rm F}\left[\theta(1-x-\delta)\frac{1+x^2}{1-x} + \delta(1-x)(2\ln\delta + \tfrac{3}{2})\right], \tag{4.4}$$

and (cf [19, 23])

$$\begin{aligned} f_{\rm q\bar q}^{\rm DIS}(x,Q^2,\mu^2) = C_{\rm F}\Bigg[&\theta(1-x-\delta)\left\{\frac{1+x^2}{1-x}\left(\ln\frac{1-x}{x} - \frac{3}{4}\right) + \frac{9}{4} + \frac{5}{4}x\right\} \\ &+ \delta(1-x)\left\{\ln^2\delta - \tfrac{3}{2}\ln\delta - \tfrac{9}{2} - 2\zeta(2)\right\}\Bigg] \\ &+ f_{\rm q\bar q}^{\overline{\rm MS}}(x,Q^2,\mu^2) \end{aligned} \tag{4.5}$$

The pole at $x = 1$ has been regulated by adopting the convention in ref [19]. The parameter δ enables us to distinguish between soft ($x > 1-\delta$) and hard ($x < 1-\delta$) gluons It is related to the quantity Δ which appears in the soft gluon factor in (2.31) via mass factorization Up to order $\alpha_{\rm S}$ the reduced parton cross section has been computed in the following way

$$\begin{aligned} &s^2\frac{{\rm d}^2\hat\sigma_{\rm q\bar q}^{(1)}(s,t_1,u_1,Q^2)}{{\rm d}t_1\,{\rm d}u_1} \\ &= s^2\frac{{\rm d}^2\sigma_{\rm q\bar q}^{(1)}(s,t_1,u_1,\mu^2,\epsilon)}{{\rm d}t_1\,{\rm d}u_1} \\ &\quad - \frac{\alpha_{\rm S}}{2\pi}\left\{\int_0^1\frac{{\rm d}x_1}{x_1}\left[P_{\rm q\bar q}(x_1)\frac{2}{\epsilon} + f_{\rm q\bar q}(x_1,Q^2,\mu^2)\right]\hat s^2\frac{{\rm d}^2\sigma_{\rm q\bar q}^{(0)}(x_1 s, x_1 t_1, u_1)}{{\rm d}\hat t_1\,{\rm d}u_1}\right. \\ &\quad \left. + \int_0^1\frac{{\rm d}x_2}{x_2}\left[P_{\rm q\bar q}(x_2)\frac{2}{\epsilon} + f_{\rm q\bar q}(x_2,Q^2,\mu^2)\right]\hat s^2\frac{{\rm d}^2\sigma_{\rm q\bar q}^{(0)}(x_2 s, t_1, x_2 u_1)}{{\rm d}t_1\,{\rm d}\hat u_1}\right\}. \end{aligned} \tag{4.6}$$

Using the Born cross section ${\rm d}\sigma_{\rm q\bar q}^{(0)}$ in eq. (2.5) and the parton cross section ${\rm d}\sigma_{\rm q\bar q}^{(1)}$

in sect. 2 we get the following results. Like $d\sigma_{q\bar{q}}^{(1)}$ the reduced parton cross section $d\hat{\sigma}_{q\bar{q}}^{(1)}$ can be split into a virtual plus soft (V + S) and a hard gluon (H) part. The virtual plus soft gluon part of the reduced cross section can be written as

$$\left(d\hat{\sigma}_{q\bar{q}}^{(1)}\right)^{V+S} = \left(d\hat{\sigma}_{q\bar{q},F}^{(1)}\right)^{V+S} + \left(d\hat{\sigma}_{q\bar{q},A}^{(1)}\right)^{V+S} + \left(d\hat{\sigma}_{q\bar{q},f}^{(1)}\right)^{V}. \tag{4.7}$$

The expressions for $(d\hat{\sigma}_{q\bar{q},F}^{(1)})^{V+S}$ and $(d\hat{\sigma}_{q\bar{q},A}^{(1)})^{V+S}$ are rather long and will be presented in appendix A. They can be split into a symmetric and an antisymmetric part with respect to the interchange of t_1 and u_1. The sum and difference of these two parts represent the production cross sections for a detected heavy antiquark and a detected heavy quark, respectively.

The fermion loop contribution $(d\hat{\sigma}_{q\bar{q},f}^{(1)})^{V}$ does not need any mass factorization and hence its result can be found in eq. (2.15). Notice that like in the gluon–gluon fusion process the F part of the virtual plus soft cross section behaves near threshold (i.e. $s \to 4m^2$) as $\pi^2/\bar{s}$ where $\bar{s} = s\sqrt{1-4m^2/s}$. This implies that the total parton cross section goes to a constant in the threshold limit. This effect can be attributed to the Coulomb singularity caused by the exchange of massless gauge bosons between massive fermions and originates from the vertex correction graph in fig. 2e.

The hard gluon reduced cross section is equal to the sum of the following parts [see eq. (2.20)]

$$\begin{aligned}\left(s^2\frac{d^2\hat{\sigma}_{q\bar{q},F}^{(1)}}{dt_1\,du_1}\right)_{\overline{MS}}^{H} &= \tfrac{1}{2}\alpha_s^3 K_{q\bar{q}} N C_F^2\left[\left[\left\{\ln\frac{s_4^2}{m^2(s_4+m^2)} + \ln\frac{m^2}{Q^2}\right\}\right.\right.\\
&\quad\times\left\{-\frac{1}{u_1}\left(\frac{u_1^2+(s+t_1)^2}{s_4(s+t_1)}\right)\left(\frac{t_1^2+(s+t_1)^2}{s^2} - \frac{2m^2(s+t_1)}{u_1 s}\right)\right\}\\
&\quad\left.\left.-\frac{s_4}{u_1(s+t_1)}\left(\frac{t_1^2+(s+t_1)^2}{s^2} - \frac{2m^2(s+t_1)}{u_1 s}\right)\right] + (t_1 \leftrightarrow u_1)\right]\\
&\quad+\left(\frac{1}{2}\right)^5\frac{\alpha_s^3}{\pi}K_{q\bar{q}} N C_F^2\frac{s_4}{s_4+m^2}\left(\int d\Omega_n\,R_F\right)^{\text{finite}},\end{aligned} \tag{4.8}$$

$$\left(s^2\frac{d^2\hat{\sigma}_{q\bar{q},A}^{(1)}}{dt_1\,du_1}\right)_{\overline{MS}}^{H} = \left(\frac{1}{2}\right)^5\frac{\alpha_s^3}{\pi}K_{q\bar{q}} N C_A C_F\frac{s_4}{s_4+m^2}\left(\int d\Omega_4\,R_A\right). \tag{4.9}$$

As has been mentioned below (2.22) the A part does not need any mass factorization. The expressions for $(\ )^{\text{finite}}$ are too long to be presented in this article. They can be found in our Fortran program and are available upon request Like in the virtual plus soft (reduced) cross section (see appendix A) the second term in eq. (4 8) and expression (4 9) can be split into a symmetric and an antisymmetric part. In the case that the heavy antiquark is detected we have

$$\frac{s_4}{s_4+m^2}\left(\int \mathrm{d}\Omega_n\, R_{\mathrm{F}}\right)_{\bar{\mathrm{Q}}}^{\mathrm{finite}} = S_{\mathrm{QQF}}(s,t_1,u_1) + A_{\mathrm{QQF}}(s,t_1,u_1)\,, \tag{4.10}$$

$$\frac{s_4}{s_4+m^2}\left(\int \mathrm{d}\Omega_4\, R_{\mathrm{A}}\right)_{\bar{\mathrm{Q}}} = S_{\mathrm{QQA}}(s,t_1,u_1) + A_{\mathrm{QQA}}(s,t_1,u_1)\,, \tag{4 11}$$

where $S_{\mathrm{QQF}}, S_{\mathrm{QQA}}$ are symmetric whereas $A_{\mathrm{QQF}}, A_{\mathrm{QQA}}$ are antisymmetric with respect to the interchange of t_1 and u_1 Here t_1 and u_1 denote the square of the four-momentum transfer of the detected heavy antiquark with respect to the incoming light antiquark and quark respectively If we detect the heavy quark in the final state the production cross sections for the latter are given as follows. The first part of the expression (4 8) remains unchanged The second part of (4 8) becomes

$$\frac{s_4}{s_4+m^2}\left(\int \mathrm{d}\Omega_n\, R_{\mathrm{F}}\right)_{\mathrm{Q}}^{\mathrm{finite}} = S_{\mathrm{QQF}}(s,t_1,u_1) - A_{\mathrm{QQF}}(s,t_1,u_1)\,, \tag{4.12}$$

and expression (4.9) now reads

$$\frac{s_4}{s_4+m^2}\left(\int \mathrm{d}\Omega_4\, R_{\mathrm{A}}\right)_{\mathrm{Q}} = S_{\mathrm{QQA}}(s,t_1,u_1) - A_{\mathrm{QQA}}(s,t_1,u_1) \tag{4.13}$$

It is clear from the above remarks that the expressions (4 12) and (4 13) can be derived by interchanging t_1 and u_1 in (4 10) and (4 11), where in the definitions of t_1 and u_1 the role of the heavy antiquark is now taken by the detected heavy quark Finally we want to mention that replacement of the heavy antiquark by the heavy quark is the same as interchanging the role of the incoming light quark and light antiquark with respect to t_1 and u_1.

While going from the $\overline{\mathrm{MS}}$ to the DIS scheme one has to add the following expressions to (4 7) and (4 8)

$$\left(s^2\frac{\mathrm{d}^2\hat{\sigma}^{(1)}_{q\bar{q},\mathrm{F}}}{\mathrm{d}t_1\,\mathrm{d}u_1}\right)^{\mathrm{V+S}}_{\mathrm{DIS}} = \left(s^2\frac{\mathrm{d}^2\hat{\sigma}^{(1)}_{q\bar{q},\mathrm{F}}}{\mathrm{d}t_1\,\mathrm{d}u_1}\right)^{\mathrm{V+S}}_{\overline{\mathrm{MS}}} + \tfrac{1}{2}\alpha_s^3 K_{q\bar{q}} N C_{\mathrm{F}}^2\left[\left(-\ln^2\frac{\Delta}{s+t_1}\right.\right.$$
$$\left.\left. + \tfrac{3}{2}\ln\frac{\Delta}{s+t_1} + \tfrac{9}{2} + 2\zeta(2)\right) + (t_1\leftrightarrow u_1)\right]A_{\mathrm{QED}}\delta(s_4)\,, \tag{4.14}$$

with A_{QED} defined in eq (2.4) and

$$\left(s^2\frac{d^2\hat{\sigma}^{(1)}_{q\bar{q}\,F}}{dt_1\,du_1}\right)^{H}_{DIS} = \left(s^2\frac{d^2\hat{\sigma}^{(1)}_{q\bar{q}\,F}}{dt_1\,du_1}\right)^{H}_{\overline{MS}} + \tfrac{1}{2}\alpha_S^3 K_{q\bar{q}} N C_F^2$$

$$\times\left[\frac{1}{u_1}\left\{\frac{u_1^2+(s+t_1)^2}{s_4(s+t_1)}\left(\ln\frac{s_4}{-u_1}-\frac{3}{4}\right)+\frac{9}{4}-\frac{5}{4}\frac{u_1}{s+t_1}\right\}\right.$$

$$\left.\times\left\{\frac{t_1^2+(s+t_1^2)}{s^2}-\frac{2m^2(s+t_1)}{su_1}\right\}+(t_1\leftrightarrow u_1)\right], \qquad (4.15)$$

respectively

As has been mentioned before the (anti)quark-gluon subprocess is a non-diagonal one Therefore, one has to be careful with the gluon polarization average factor which is $(n-2)^{-1}$ in n-dimensions. To render the cross section for the (anti)quark-gluon process in sect 3 finite we need the following splitting functions

$$P_{gq}(x) = C_F\left[\frac{1+(1-x)^2}{x}\right], \qquad (4.16)$$

$$P_{qg}(x) = T_f\left[x^2+(1-x)^2\right], \qquad (4.17)$$

with $T_f = 1/2$ In the DIS scheme we have the following expressions [19,23]

$$f_{gq}^{DIS}(x,Q^2,\mu^2) = f_{gq}^{\overline{MS}}(x,Q^2,\mu^2), \qquad (4.18)$$

$$f_{qg}^{DIS}(x,Q^2,\mu^2) = T_f\left[\{x^2+(1-x)^2\}\ln\frac{1-x}{x}+8x(1-x)-1\right]+f_{qg}^{\overline{MS}}(x,Q^2,\mu^2) \qquad (4.19)$$

Notice that f_{gq}^{DIS} cannot be directly calculated in deep inelastic lepton-hadron scattering However, other choices for f_{gq} are possible, e.g one can choose it in such a way that the momentum sum rule is satisfied (see refs [2,24] and appendix B). The expression for f_{gq} differs from the usual one quoted in the literature [19,23]. In the latter the factor $1/2$ was used instead of $(n-2)^{-1}$ for the gluon polarization. It turns out that this does not affect the final results given in refs. [19,23]. The reduced parton cross section for the gluon-antiquark subprocess is given by

$$s^2\frac{d^2\hat{\sigma}^{(1)}_{g\bar{q}}(s,t_1,u_1,Q^2)}{dt_1\,du_1}$$
$$= s^2\frac{d^2\sigma^{(1)}_{g\bar{q}}(s,t_1,u_1,\mu^2,\epsilon)}{dt_1\,du_1} - \frac{\alpha_S}{2\pi}\left\{\int_0^1\frac{dx_1}{x_1}\right.$$
$$\times\left[P_{qg}(x_1)\frac{2}{\epsilon}+f_{qg}(x_1,Q^2,\mu^2)\right]\hat{s}^2\frac{d^2\sigma^{(0)}_{q\bar{q}}(x_1 s, x_1 t_1, u_1)}{d\hat{t}_1\,du_1}$$
$$\left.+\int_0^1\frac{dx_2}{x_2}\left[P_{g\bar{q}}(x_2)\frac{2}{\epsilon}+f_{g\bar{q}}(x_2,Q^2,\mu^2)\right]\hat{s}^2\frac{d^2\sigma^{(0)}_{gg}(x_2 s, t_1, x_2 u_1)}{dt_1\,d\hat{u}_1}\right\} \tag{4.20}$$

The Born cross sections $d\sigma^{(0)}_{q\bar{q}}$ and $d\sigma^{(0)}_{gg}$ are given by expression (2.5) and

$$s^2\frac{d^2\sigma^{(0)}_{gg}}{dt_1\,du_1} = \alpha_S^2 K_{gq} N\frac{\pi}{(4\pi)^{\epsilon/2}}\frac{1}{(1+\epsilon/2)^2\Gamma(1+\epsilon/2)}\left(\frac{t_1u_1-sm^2}{\mu^2 s}\right)^{\epsilon/2}$$
$$\times\left[C_F - C_A\frac{t_1u_1}{s^2}\right]B_{QED}\delta(s+t_1+u_1), \tag{4.21}$$

where the factor $(1+\epsilon/2)^{-2}$ arises from the polarization average factor in n-dimensions and

$$B_{QED} = \frac{t_1}{u_1}+\frac{u_1}{t_1}+\frac{4m^2 s}{t_1u_1}\left(1-\frac{m^2 s}{t_1u_1}\right)+\epsilon\left(-1+\frac{s^2}{t_1u_1}\right)+\epsilon^2\left(\frac{s^2}{4t_1u_1}\right). \tag{4.22}$$

The gluon–antiquark reduced cross section is equal to the sum of the following expressions:

$$\left(s^2\frac{d^2\hat{\sigma}^{(1)}_{g\bar{q}\,F}}{dt_1\,du_1}\right)_{\overline{MS}} = \tfrac{1}{2}\alpha_S^3 K_{gq} N C_F^2\left[\left\{\ln\frac{s_4^2}{m^2(s_4+m^2)}+\ln\frac{m^2}{Q^2}\right\}\right.$$
$$\times\left\{\frac{s+t_1}{u_1^2}\left(\frac{s_4^2+(s+t_1)^2}{(s+t_1)^2}\right)\left(\frac{t_1^2+(s+t_1)^2}{-t_1(s+t_1)}+\frac{4m^2 s}{t_1u_1}\left(1-\frac{m^2 s}{t_1u_1}\right)\right)\right.$$
$$\left.-\frac{1}{t_1}\frac{s_4^2+t_1^2}{(s+u_1)^2}\left(\frac{(s+u_1)^2+u_1^2}{s^2}-\frac{2m^2(s+u_1)}{st_1}\right)\right\}$$
$$+\frac{s+t_1}{u_1^2}\left(\frac{s_4^2+(s+t_1)^2}{(s+t_1)^2}\right)\left(\frac{4m^2 s}{t_1u_1}\left(1-\frac{m^2 s}{t_1u_1}\right)\right)-\frac{t_1^2+(s+t_1)^2}{t_1(s+t_1)^2}$$
$$\left.+\frac{2s_4}{(s+u_1)^2}\left(\frac{(s+u_1)^2+u_1^2}{s^2}-\frac{2m^2(s+u_1)}{st_1}\right)\right]$$
$$+\left(\frac{1}{2}\right)^5\frac{\alpha_S^3}{\pi}K_{gq}NC_F^2\frac{s_4}{s_4+m^2}\left(\int d\Omega_n\,R_{g\bar{q},F}\right)^{\text{finite}}, \tag{4.23}$$

and

$$s^2\left(\frac{\mathrm{d}^2\hat{\sigma}^{(1)}_{\mathrm{g}\bar{\mathrm{q}},\mathrm{A}}}{\mathrm{d}t_1\,\mathrm{d}u_1}\right)_{\overline{\mathrm{MS}}} = \tfrac{1}{2}\alpha_s^3 K_{\mathrm{gq}} N C_{\mathrm{A}} C_{\mathrm{F}}\Bigg[\left\{\ln\frac{s_4^2}{m^2(s_4+m^2)} + \ln\frac{m^2}{Q^2}\right\}$$

$$\times\left\{\frac{t_1(s+t_1)^2}{s^2u_1^2}\left(\frac{s_4^2+(s+t_1)^2}{(s+t_1)^2}\right)\left(\frac{t_1^2+(s+t_1)^2}{-t_1(s+t_1)}+\frac{4m^2s}{t_1u_1}\left(1-\frac{m^2s}{t_1u_1}\right)\right)\right\}$$

$$+\frac{t_1(s+t_1)^2}{s^2u_1^2}\left(\frac{s_4^2+(s+t_1)^2}{(s+t_1)^2}\right)\left(\frac{4m^2s}{t_1u_1}\left(1-\frac{m^2s}{t_1u_1}\right)\right)-\frac{t_1^2+(s+t_1)^2}{s^2(s+t_1)}\Bigg]$$

$$+\left(\frac{1}{2}\right)^5\frac{\alpha_s^3}{\pi}K_{\mathrm{gq}}NC_{\mathrm{A}}C_{\mathrm{F}}\frac{s_4}{s_4+m^2}\left(\int\mathrm{d}\Omega_n\,R_{\mathrm{g}\bar{\mathrm{q}},\mathrm{A}}\right)^{\mathrm{finite}} \tag{4.24}$$

The expressions for $(\ )^{\mathrm{finite}}$ are too long to be presented here. They can be found in our computer program.

Like in the quark–antiquark subprocess the last terms of eqs. (4.23) and (4.24) can be split into a symmetric and an antisymmetric part with respect to t_1 and u_1. For the gluon–antiquark reaction we get

$$\frac{s_4}{s_4+m^2}\left(\int\mathrm{d}\Omega_n\,R_{\mathrm{g}\bar{\mathrm{q}},\mathrm{F}}\right)^{\mathrm{finite}}_{\bar{\mathrm{Q}}} = S_{\mathrm{GQF}}(s,t_1,u_1)+A_{\mathrm{GQF}}(s,t_1,u_1), \tag{4.25}$$

$$\frac{s_4}{s_4+m^2}\left(\int\mathrm{d}\Omega_n\,R_{\mathrm{g}\bar{\mathrm{q}},\mathrm{A}}\right)^{\mathrm{finite}}_{\bar{\mathrm{Q}}} = S_{\mathrm{GQA}}(s,t_1,u_1)+A_{\mathrm{GQA}}(s,t_1,u_1), \tag{4.26}$$

where S_{GQF}, S_{GQA} are symmetric whereas A_{GQF}, A_{GQA} are antisymmetric with respect to the interchange of t_1 and u_1. Here t_1 and u_1 denote the squares of the four-momentum transfers of the outgoing heavy antiquark with respect to the light incoming antiquark and the gluon respectively. Analogous to the gluon–antiquark reaction the matrix element for gluon–quark scattering can be obtained from the one calculated for the quark–antiquark process (2.16) via crossing, i.e. $k_2 \leftrightarrow -k_3$ and adding an overall minus sign to the square of the amplitude.

This implies that the invariants listed in eq. (2.17), which appear in the squared amplitude $\Sigma M_{\mathrm{gq}} M^*_{\mathrm{gq}}$, are obtained from those present in $\Sigma M^{\mathrm{R}} M^{\mathrm{R}*}$ in eq. (2.18) via the following replacements, $s \leftrightarrow u'$, $s_3 \leftrightarrow t_1$, $s_4 \leftrightarrow u_6$. Notice that in the gluon–quark subprocess t_1 and u_1 denote the momentum transfers of the heavy antiquark with respect to the gluon and the light quark respectively.

The gluon–quark cross section can be obtained from the gluon–antiquark one by interchanging t_1 and u_1 in the first parts of expressions (4.23) and (4.24). The second parts of these equations can be written as [see eqs (4.25) and (4 26)]

$$\frac{s_4}{s_4+m^2}\left(\int \mathrm{d}\Omega_n\, R_{\mathrm{gq,F}}\right)_{\bar{\mathrm{Q}}}^{\mathrm{finite}} = S_{\mathrm{GQF}}(s,t_1,u_1) - A_{\mathrm{GQF}}(s,t_1,u_1)\,, \quad (4\,27)$$

$$\frac{s_4}{s_4+m^2}\left(\int \mathrm{d}\Omega_n\, R_{\mathrm{gq\,A}}\right)_{\bar{\mathrm{Q}}}^{\mathrm{finite}} = S_{\mathrm{GQA}}(s,t_1,u_1) - A_{\mathrm{GQA}}(s,t_1,u_1) \quad (4\,28)$$

If the final state heavy antiquark is replaced by a heavy quark the cross sections for the latter process can be derived from the former via the relation

$$\left(s^2\frac{\mathrm{d}^2\hat{\sigma}^{(1)}}{\mathrm{d}t_1\,\mathrm{d}u_1}\right)_{\mathrm{g\bar{q}}\to\mathrm{Q}} = \left(s^2\frac{\mathrm{d}^2\hat{\sigma}^{(1)}}{\mathrm{d}t_1\,\mathrm{d}u_1}\right)_{\mathrm{gq}\to\bar{\mathrm{Q}}}, \quad (4\,29)$$

$$\left(s^2\frac{\mathrm{d}^2\hat{\sigma}^{(1)}}{\mathrm{d}t_1\,\mathrm{d}u_1}\right)_{\mathrm{gq}\to\mathrm{Q}} = \left(s^2\frac{\mathrm{d}^2\hat{\sigma}^{(1)}}{\mathrm{d}t_1\,\mathrm{d}u_1}\right)_{\mathrm{g\bar{q}}\to\bar{\mathrm{Q}}}, \quad (4\,30)$$

where in the definitions of t_1 and u_1 the role of the heavy antiquark is now taken by the detected heavy quark

The reduced cross sections in the DIS scheme are given by

$$\left(s^2\frac{\mathrm{d}^2\sigma^{(1)}_{\mathrm{g\bar{q}}\,\mathrm{F}}}{\mathrm{d}t_1\,\mathrm{d}u_1}\right)_{\mathrm{DIS}} = \left(s^2\frac{\mathrm{d}^2\hat{\sigma}^{(1)}_{\mathrm{g\bar{q}},\mathrm{F}}}{\mathrm{d}t_1\,\mathrm{d}u_1}\right)_{\overline{\mathrm{MS}}} + \tfrac{1}{2}\alpha_{\mathrm{S}}^3 K_{\mathrm{gq}} N C_{\mathrm{F}}^2\left[\frac{1}{t_1}\left\{\frac{s_4^2+t_1^2}{(s+u_1)^2}\ln\frac{s_4}{-t_1}\right.\right.$$
$$\left.\left. - \frac{8t_1 s_4}{(s+u_1)^2} - 1\right\}\left\{\frac{(s+u_1)^2+u_1^2}{s^2} - \frac{2m^2(s+u_1)}{st_1}\right\}\right] \quad (4\,31)$$

Before finishing this section we would like to stress that the part of the matrix element leading to the asymmetry in t_1 and u_1 never contributes to the collinear divergences. This holds for the collinear divergences in the initial state ($1/\epsilon$ poles) as well as in the final state (when $m \to 0$) Since the first parts of eqs (4.8), (4 23) and (4 24) are remnants of the initial state collinear divergences they will be unaltered (apart from the $t_1 \leftrightarrow u_1$ interchange) when the quarks are replaced by antiquarks irrespective of whether this occurs in the initial or the final state. The same applies to the extra terms needed to go from the $\overline{\mathrm{MS}}$ to the DIS scheme [see eqs. (4 14), (4.15) and (4.31)].

5. Parton–parton cross sections

Before presenting the results for the hadronic distributions we first discuss the parton–parton cross sections and compare them with those already presented in the literature [2]. The total cross section is defined by

$$\hat{\sigma}_{ij}(s,m^2) = \int_{(s-\tilde{s})/2}^{(s+\tilde{s})/2} \mathrm{d}(-t_1) \int_{-m^2 s/t_1}^{s+t_1} \mathrm{d}(-u_1) \frac{\mathrm{d}^2\hat{\sigma}_{ij}(s,t_1,u_1,Q^2)}{\mathrm{d}t_1\,\mathrm{d}u_1}, \quad (5.1)$$

where $\tilde{s} = s\sqrt{1-4m^2/s}$. When we have a gluon in the final state we follow the procedure in ref. [4] and split the cross section in a hard (H) and a virtual plus soft (V + S) part. The latter is obtained from the expressions in eqs. (2.15), (4.7) and (A.1), (A.2) by removing the $\ln \Delta/m^2$ terms. These terms are added to the hard cross section so that the latter will become independent of $\ln \Delta$ when $\Delta \to 0$. If we exclude the fermion loop contribution we can express the perturbative expansion of the parton–parton cross section in terms of scaling functions [2], i.e.

$$\hat{\sigma}_{ij}(s,m^2) = \frac{\alpha_s^2}{m^2}\left[f_{ij}^{(0)}(\eta) + 4\pi\alpha_s\left\{f_{ij}^{(1)}(\eta) + \bar{f}_{ij}^{(1)}(\eta)\ln\frac{Q^2}{m^2}\right\}\right], \quad (5.2)$$

where $f_{ij}^{(0)}(\eta)$, $f_{ij}^{(1)}(\eta)$ stand for the Born contribution and the order α_s correction respectively and $\eta = s/4m^2 - 1$. The function $\bar{f}_{ij}^{(1)}(\eta)$ shows up if the mass factorization scale Q^2 deviates from the heavy flavour mass m^2. Since the fermion loop contribution depends on the internal flavour mass m_i it cannot be expressed as a scaling function in η. However if one chooses a renormalization scheme where the heavy flavour quarks are decoupled in the limit of small momenta scaling will be restored provided the following conditions are satisfied.

First, all flavours lighter than the produced one are taken to be light quarks and their mass is set equal to zero. Second, the sum over the internal heavy flavours in eq. (2.15) only includes the contribution of the quark which is produced in the final state.

In fig. 4 we have plotted $f_{q\bar{q}}^{(0)}(\eta)$ and $f_{q\bar{q}}^{(1)}(\eta)$ for the $\overline{\mathrm{MS}}$ scheme. The latter quantity has been split in a hard and a virtual plus soft gluon part. The fermion loop contribution has been included in the virtual part where we have chosen four light flavours and one heavy quark (this holds for bottom pair production). From fig. 4 we infer that for $\eta < 0.01$ the order α_s correction dominates the zeroth order one, bearing in mind that for the cross section $f_{q\bar{q}}^{(1)}(\eta)$ has to be multiplied by $4\pi\alpha_s$. This effect can be attributed to the soft gluon terms of the type $s_4^{-1}\ln^i s_4/m^2$ which are present in the hard gluon part of the cross sections in eqs. (4.8) and (4.9). Another feature is that the function $f_{q\bar{q}}^{(1)}(\eta)$ becomes negative in the region $0.7 < \eta < 20$. This region is very important for the hadronic cross section as we have mentioned in sect. 1.

At threshold the virtual plus soft piece contains a large contribution from the π^2 terms discussed below eq. (4.7). This term originates from the Coulomb singularity present in the vertex correction graph in fig. 2e. Near threshold $\eta \to 0$ the

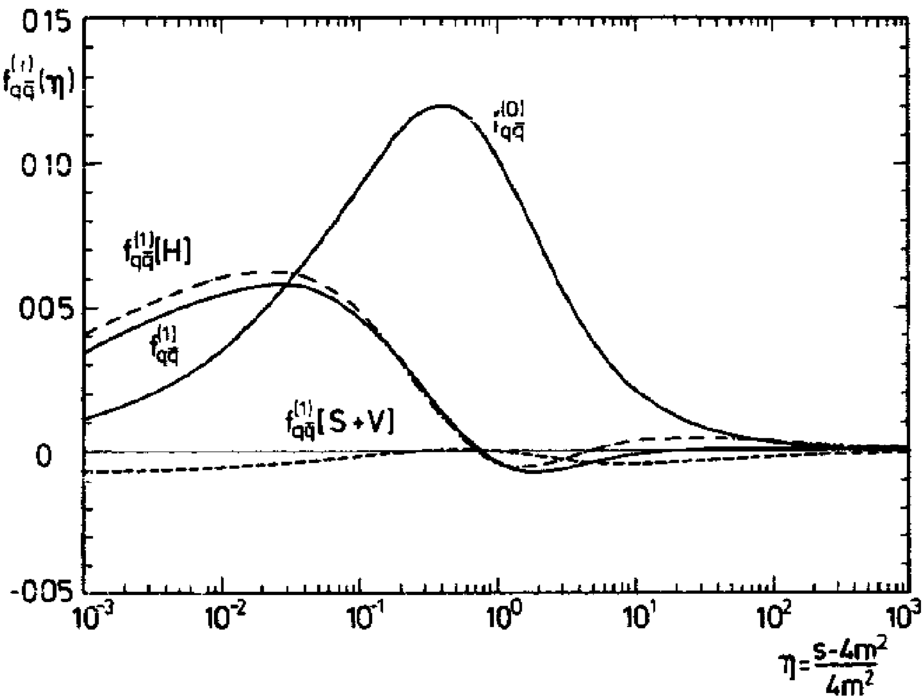

Fig 4 The quark–antiquark scaling functions from our exact order α_S^3 calculations in the $\overline{\mathrm{MS}}$ scheme $f^{(0)}_{q\bar{q}}$ and $f^{(1)}_{q\bar{q}}$ are defined in eq (5 2) and plotted as solid lines versus $\eta = (s - 4m^2)/4m^2$ The soft plus virtual contributions $f^{(1)}_{q\bar{q}}[S+V]$ (see sect 5) with $\log \Delta/m^2$ terms removed is represented by the dashed line The sum of the hard and the $\log \Delta/m^2$ contributions $f^{(1)}_{q\bar{q}}[H]$ is represented by the dash–dotted line

parton–parton cross section can be exactly calculated from the expressions given in eqs (A 1) and (A.2) because there exists a one-to-one correspondence between the $s_4^{-1} \ln^i s_4/m^2$ terms in $\hat{\sigma}^{H}_{q\bar{q}}$ and the $\ln^{i+1} \Delta/m^2$ terms in $\hat{\sigma}^{V+S}_{q\bar{q}}$ In the limit $s \to 4m^2$ we obtain

$$\hat{\sigma}_{q\bar{q}}(s, m^2)|_{\overline{\mathrm{MS}}} = \pi\alpha_S^2 K_{q\bar{q}} \frac{1}{s}\left[NC_F\beta + \frac{\alpha_S}{\pi}NC_F^2\left\{\frac{\pi^2}{2} + 2\beta\ln^2(8\beta^2)\right.\right.$$
$$\left.\left. -8\beta\ln(8\beta^2) - 2\beta\ln\frac{Q^2}{m^2}\ln(4\beta^2)\right\} + \frac{\alpha_S}{\pi}NC_A C_F\left\{-\frac{\pi^2}{4} - \beta\ln(8\beta^2)\right\}\right], \quad (5\ 3)$$

with $\beta = \sqrt{1 - 4m^2/s}$ In the case of QCD ($N = 3$) the above expression agrees with that given in eq (2.6) of ref [2] It describes the threshold behaviour of $\hat{\sigma}_{q\bar{q}}$ very well for values of $\eta < 0.001$. Notice that the large corrections near threshold can be resummed since the leading part exponentiates like $\exp(2\alpha_S C_F(\ln^2 8\beta^2)/\pi)$, cf. ref. [25]. In fig 5 we show the difference in the behaviour of $f^{(1)}_{q\bar{q}}$ in the $\overline{\mathrm{MS}}$ and the DIS schemes. Adopting the DIS scheme still yields a negative contribution in $0.7 < \eta < 20$. Moreover we also plotted the mass factorization part $\bar{f}^{(1)}_{q\bar{q}}$ in (5.2) In

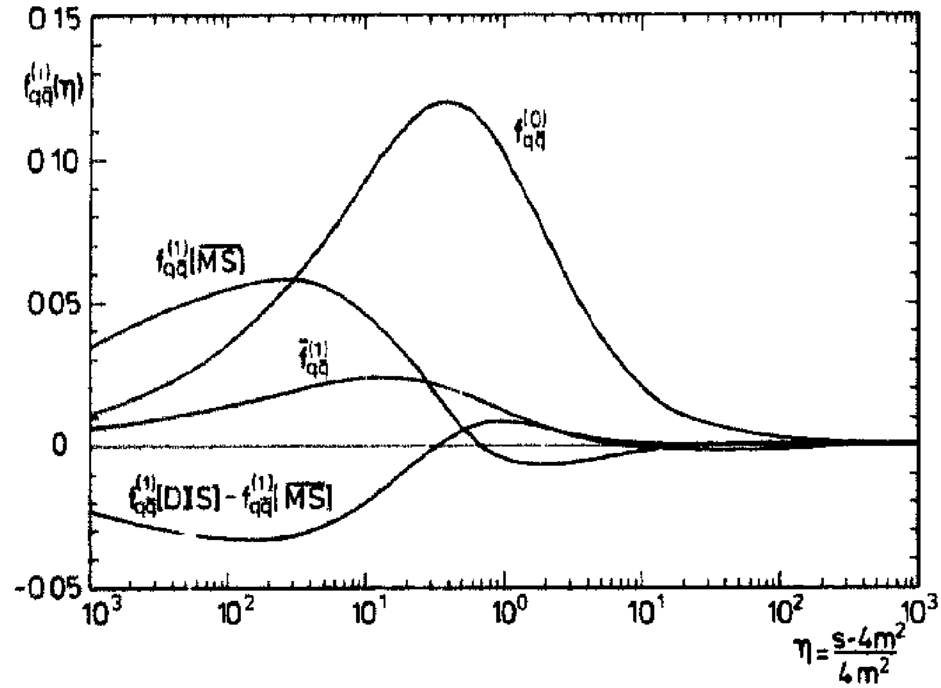

Fig 5. The exact results for the quark–antiquark scaling functions in the $\overline{MS}$ scheme The difference $f^{(1)}_{q\bar{q}}[DIS]-f^{(1)}_{q\bar{q}}[\overline{MS}]$ is also plotted here

the case of $f^{(1)DIS}_{q\bar{q}}-f^{(1)\overline{MS}}_{q\bar{q}}$ and $\bar{f}^{(1)}_{q\bar{q}}$ we observe the same features as in $f^{(1)\overline{MS}}_{q\bar{q}}$ except for the π^2 term mentioned above which does not show up here. The threshold behaviour of the contribution of $\bar{f}^{(1)}_{q\bar{q}}$ to the cross section has already been shown in eq (5.3). The difference between the DIS and the $\overline{MS}$ scheme for $s \to 4m^2$ is given by

$$\hat{\sigma}_{q\bar{q}}(s, m^2)|_{DIS} - \hat{\sigma}_{q\bar{q}}(s, m^2)|_{\overline{MS}} = \alpha_s^3 K_{q\bar{q}} \frac{1}{s} N C_F^2 \beta\left[-\ln^2 4\beta^2 + \tfrac{11}{2}\ln 4\beta^2\right], \quad (5.4)$$

which agrees with eq (40) in ref. [2] provided the same limit has been taken.

In fig 6 we have made similar plots for the gluon–quark reaction. Here we used the DIS scheme as defined in appendix B, which implements the momentum sum rule for the gluon structure functions. We will continue to use this scheme for all the results in this article. We have however checked that the difference between the two DIS schemes mentioned in the text is extremely small in this channel. The large plateau behaviour of the functions $f^{(1)\overline{MS}}_{gq}$ and $\bar{f}^{(1)}_{gq}$ for $\eta > 100$ can be attributed to the gluon splitting and flavour excitation mechanisms (see refs. [3, 4]) in the gluon–quark channel. This effect can be explained by the exchange of a gluon in the t-channel of the subprocess $q + g \to q + g^*$ where $g^* \to Q + \bar{Q}$ (gluon splitting) and $g \to \bar{q} + q^*$ where $q^* + \bar{q} \to Q + \bar{Q}$ (flavour excitation). Both subprocesses dominate the cross section $\hat{\sigma}_{gq}$ in the high-energy limit [2, 9]. In fig. 6 we

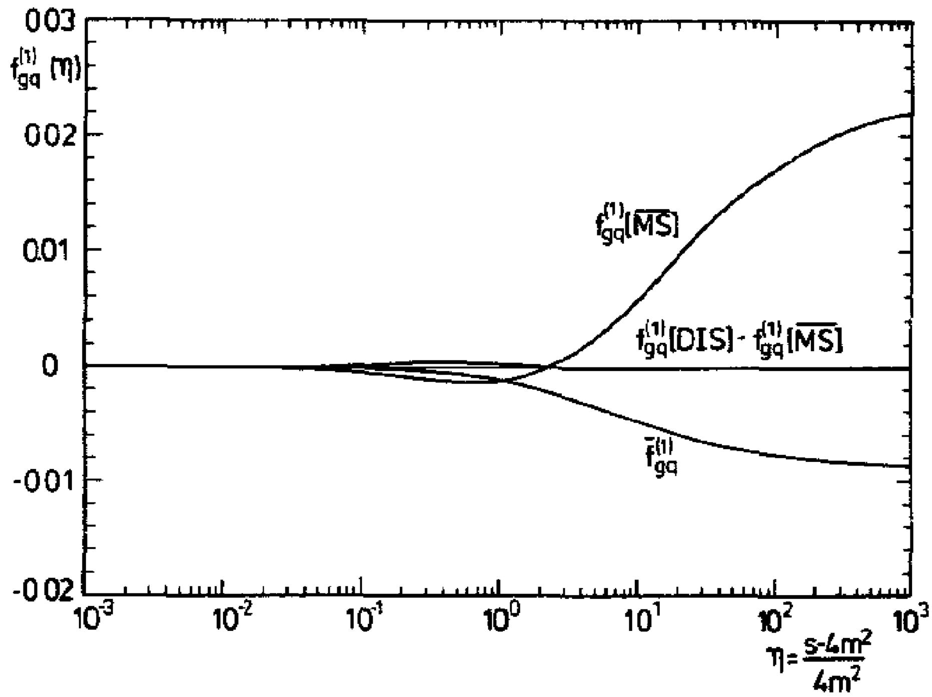

Fig 6 The exact results for the gluon–quark or gluon–antiquark scaling functions $f^{(1)}_{gq}[\overline{MS}]$, $\bar{f}^{(1)}_{gq}$ and the difference $f^{(1)}_{gq}[DIS] - f^{(1)}_{gq}[\overline{MS}]$ where the momentum sum rule is imposed

also show the difference $f^{(1)DIS}_{gq} - f^{(1)\overline{MS}}_{gq}$ which turns out to be very small. Notice that in our case $f^{(1)DIS}_{gq} - f^{(1)\overline{MS}}_{gq}$ is derived from the deep inelastic Wilson coefficient in eq. (4.19) (see also eq. (4.20) in ref [3]) and not from (3.7) of ref [2]. We remark that the parton–parton cross section $\sigma^{(1)}_{gq}$ which is positive before mass factorization becomes negative when the collinear divergences are subtracted (see the region $0.02 < \eta < 2$ in fig 6) Like in the $q\bar{q}$ annihilation process this region is very important for the hadronic cross section

The functions f_{ij}, $\bar{f}_{ij}$ have already been presented in ref [2] and they agree with ours. To further check that there are no differences between the two calculations at this level we have also computed the rapidity distribution of the heavy quark and antiquark We obtained the subroutines listed in the appendix of ref. [3] from P. Nason and linked them to our own Monte Carlo programs. The comparison has been made in the case where the differential distributions are calculated in the $\overline{MS}$ scheme The transitions from the $\overline{MS}$ to the DIS scheme as expressed in eqs (4.14), (4.15), (4.31) and appendix B have only been checked analytically. They agree with those presented in sect 4 of ref. [3]. The results for the rapidity distribution of the heavy antiquark in the reaction $k_1 + k_2 \to \overline{Q} + X$, where k_1 and k_2 represent the incoming partons, are given in fig. 7 for $\sqrt{s} = 100$ GeV, $m_b = 5$ GeV/c^2 and $n_f = 5$. The rapidity y is defined to be positive when the momenta of k_1 and $\overline{Q}$ are parallel. At $\sqrt{s} = 100$ GeV, $m_b = 5$ GeV/c^2 the $q\bar{q}$ contribution becomes very small so that we have multiplied the $q\bar{q}$ contribution in this plot by a

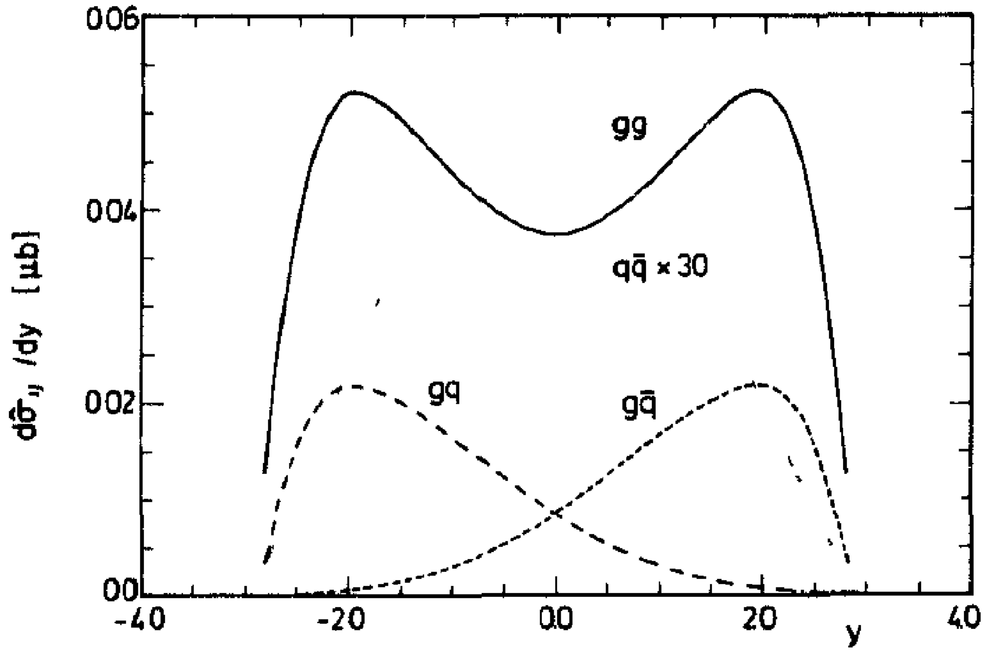

Fig 7 The exact order α_s^3 parton–parton differential cross section in the rapidity of the outgoing heavy antiquark, $d\sigma_{ij}/dy$ in the $\overline{\rm MS}$ scheme The rapidity y is defined in the c m frame of the incoming partons and we use $\mu_R = Q = m_Q = 5$ GeV/c^2, $\sqrt{s} = 100$ GeV, $n_f = 5$ and a constant $\alpha_s = 0.25$

factor of 30, to make it more visible. The asymmetry in the rapidity distribution in the $q\bar{q}$ channel is clearly seen in this plot. There is obviously a much larger asymmetry in the qg and $\bar{q}$g channels As expected the gg contribution is symmetric. These tests show numerical agreement between the two calculations at the level of three significant places.

6. Hadron–hadron cross sections

The hadronic reaction in which heavy flavours are produced will be denoted by

$$H_1(P_1) + H_2(P_2) \to Q(p_1)(\overline{Q}(p_2)) + X, \qquad (6.1)$$

where H_1 and H_2 represent the incoming hadrons and X stands for all the final hadronic states which we sum over so that the above process is inclusive with respect to the outgoing hadrons. Since we have calculated the corrections to the single-particle inclusive reaction only, the $Q(p_1)$ or the $\overline{Q}(p_2)$ is detected. Analogous to the parton variables s, t_1 and u_1, we introduce the following invariants

$$S = (P_1 + P_2)^2, \qquad T_Q = (P_2 - p_1)^2 - m^2, \qquad U_Q = (P_1 - p_1)^2 - m^2,$$

$$T_{\overline{Q}} = (P_2 - p_2)^2 - m^2, \qquad U_{\overline{Q}} = (P_1 - p_2)^2 - m^2, \qquad (6.2)$$

Here S denotes the collider c.m. energy squared whereas T_{Q} and U_{Q} stand for the square of the four-momentum transfers of the detected heavy quark Q with respect to the hadrons H_2 and H_1, respectively. If the heavy antiquark $\overline{\mathrm{Q}}$ is detected then $T_{\overline{\mathrm{Q}}}$ and $U_{\overline{\mathrm{Q}}}$ are the square of the four-momentum transfers of the detected heavy antiquark with respect to the hadrons H_2 and H_1 respectively. The single-particle inclusive hadronic cross section is given by

$$S^2\frac{\mathrm{d}^2\sigma(S,T_1,U_1)}{\mathrm{d}T_1\,\mathrm{d}U_1}=\sum_{i,j}\int_{x_{1-}}^{1}\frac{\mathrm{d}x_1}{x_1}\int_{x_{2-}^*}^{1}\frac{\mathrm{d}x_2}{x_2}H_{ij}(x_1,x_2,Q^2)s^2\frac{\mathrm{d}^2\hat{\sigma}_{ij}(s,t_1,u_1,Q^2)}{\mathrm{d}t_1\,\mathrm{d}u_1}, \tag{6.3}$$

where Q^2 represents the factorization scale which has been set equal to the renormalization scale μ_{R}^2 The variables T_1 and U_1 stand for $T_{\mathrm{Q}}, U_{\mathrm{Q}}$ or $T_{\overline{\mathrm{Q}}}, U_{\overline{\mathrm{Q}}}$ depending whether the Q or the $\overline{\mathrm{Q}}$ is detected. The hadronic kinematical variables S, T_1 and U_1 are related to the partonic analogues s, t_1 and u_1 as follows

$$\begin{aligned}
&s=x_1x_2S,\\
&t_1=x_2T_1\,; \qquad u_1=x_1U_1 \quad \text{if } k_1=x_1P_1\,; \qquad k_2=x_2P_2\\
&t_1=x_1U_1\,; \qquad u_1=x_2T_1 \quad \text{if } k_1=x_2P_2\,, \qquad k_2=x_1P_1\,,
\end{aligned} \tag{6.4}$$

where k_1, k_2 are the incoming parton momenta as defined in eqs (2 16) and (3 1). The above relations are derived for $\overline{\mathrm{Q}}$ but they also apply to Q since in the latter case the role of p_2 in t_1 and u_1 is taken over by p_1. If $t_1=x_1T_1$ and $u_1=x_2U_1$ then the lower boundaries x_{1-} and x_{2-}^* are defined by

$$x_{1-}=\frac{-U_1}{S+T_1}\,; \qquad x_{2-}^*=\frac{\Delta-x_1T_1}{x_1S+U_1}, \tag{6.5}$$

where the cut-off parameter Δ, cf. eq. (2 27), is only relevant if the hard gluon cross section is computed. After integration over x_2 one obtains $\ln^i \Delta/m^2$ terms which have to be cancelled against the corresponding terms appearing in the soft plus virtual gluon cross section This happens for instance in the reaction $\mathrm{g}+\mathrm{g}\to \mathrm{Q}(\overline{\mathrm{Q}})+\mathrm{X}$ or in $\mathrm{q}+\bar{\mathrm{q}}\to\mathrm{Q}(\overline{\mathrm{Q}})+\mathrm{X}$ calculated up to the first order in $\alpha_{\mathrm{S}}(Q^2)$. Here $\alpha_{\mathrm{S}}(Q^2)$ now denotes the running coupling constant. The quantity H_{ij} in eq (6.3) is the product of the scale-dependent parton distribution functions. It is given by

$$H_{ij}(x_1,x_2,Q^2)=f_i^{\mathrm{H}_1}(x_1,Q^2)f_j^{\mathrm{H}_2}(x_2,Q^2)\,. \tag{6.6}$$

In the case of the gg subprocess the combination of the parton distribution functions is very simple (see e.g. eq. (7.4) in ref. [4]) However for the $\mathrm{q}\bar{\mathrm{q}}$ or $\mathrm{gq}(\bar{\mathrm{q}})$

subprocesses one has to be careful about the asymmetry in t_1 and u_1 appearing in the corresponding parton–parton cross sections. If the heavy quark is detected the cross section (6.3) takes the following form

$$
\begin{aligned}
\mathrm{d}\sigma_{\mathrm{H}_1\mathrm{H}_2\to\mathrm{Q}}(S,T_{\mathrm{Q}},U_{\mathrm{Q}}) = \int_{x_{1-}}^{1}\frac{\mathrm{d}x_1}{x_1}\int_{x_{2-}^{*}}^{1}\frac{\mathrm{d}x_2}{x_2}\Big[& f_{\mathrm{g}}^{\mathrm{H}_1}(x_1)f_{\mathrm{g}}^{\mathrm{H}_2}(x_2)\,\mathrm{d}\hat{\sigma}_{\mathrm{gg}\to\mathrm{Q}}(x_2T_{\mathrm{Q}},x_1U_{\mathrm{Q}}) \\
& + \sum_{\mathrm{q},\bar{\mathrm{q}}}\big\{f_{\mathrm{q}}^{\mathrm{H}_1}(x_1)f_{\bar{\mathrm{q}}}^{\mathrm{H}_2}(x_2)\,\mathrm{d}\hat{\sigma}_{\mathrm{q}\bar{\mathrm{q}}\to\mathrm{Q}}(x_2T_{\mathrm{Q}},x_1U_{\mathrm{Q}}) \\
& + f_{\bar{\mathrm{q}}}^{\mathrm{H}_1}(x_1)f_{\mathrm{q}}^{\mathrm{H}_2}(x_2)\,\mathrm{d}\hat{\sigma}_{\mathrm{q}\bar{\mathrm{q}}\to\mathrm{Q}}(x_1U_{\mathrm{Q}},x_2T_{\mathrm{Q}})\big\} \\
& + \sum_{\mathrm{q}}\big\{f_{\mathrm{g}}^{\mathrm{H}_1}(x_1)f_{\mathrm{q}}^{\mathrm{H}_2}(x_2)\,\mathrm{d}\hat{\sigma}_{\mathrm{gq}\to\mathrm{Q}}(x_1U_{\mathrm{Q}},x_2T_{\mathrm{Q}}) \\
& + f_{\mathrm{q}}^{\mathrm{H}_1}(x_1)f_{\mathrm{g}}^{\mathrm{H}_2}(x_2)\,\mathrm{d}\hat{\sigma}_{\mathrm{gq}\to\mathrm{Q}}(x_2T_{\mathrm{Q}},x_1U_{\mathrm{Q}})\big\} \\
& + \sum_{\bar{\mathrm{q}}}\big\{f_{\mathrm{g}}^{\mathrm{H}_1}(x_1)f_{\bar{\mathrm{q}}}^{\mathrm{H}_2}(x_2)\,\mathrm{d}\hat{\sigma}_{\mathrm{g}\bar{\mathrm{q}}\to\mathrm{Q}}(x_2T_{\mathrm{Q}},x_1U_{\mathrm{Q}}) \\
& + f_{\bar{\mathrm{q}}}^{\mathrm{H}_1}(x_1)f_{\mathrm{g}}^{\mathrm{H}_2}(x_2)\,\mathrm{d}\hat{\sigma}_{\mathrm{g}\bar{\mathrm{q}}\to\mathrm{Q}}(x_1U_{\mathrm{Q}},x_2T_{\mathrm{Q}})\big\}\Big]
\end{aligned}
\qquad (6.7)
$$

In this equation we have suppressed all variables not relevant for the asymmetry. The formula for the case that the heavy antiquark is detected can be obtained from eq. (6.7) by an overall replacement $\mathrm{Q}\to\bar{\mathrm{Q}}$. Notice that $\mathrm{d}\hat{\sigma}_{ij\to\mathrm{Q}}(t_1,u_1)\neq \mathrm{d}\hat{\sigma}_{ij\to\bar{\mathrm{Q}}}(t_1,u_1)$ which implies that the differential hadronic cross section for detected heavy quarks differs from that obtained for detected heavy antiquarks. The total hadronic cross sections are however the same.

From the differential cross section in eq. (6.3) one can derive experimentally more interesting distributions like $\mathrm{d}^2\sigma/\mathrm{d}y\,\mathrm{d}p_t$ or $\mathrm{d}^2\sigma/\mathrm{d}x_{\mathrm{F}}\,\mathrm{d}p_t$. Here y denotes rapidity, p_t the transverse momentum and $x_{\mathrm{F}}=p_l/p_{l\,\max}$ is the longitudinal momentum fraction of the outgoing heavy flavour with respect to the incoming hadron in the hadron–hadron c.m. frame.

Before discussing the results we would like to make a comment on the numerical stability of our computer program and the correctness of the boundaries listed in eq. (6.5). As one can infer from (5.1) and (6.3) there are two different ways to obtain the total hadronic cross section. The first one proceeds via the total parton cross section in eq. (5.1) by convoluting it with the total parton–parton flux (see eq. (7.14) in ref. [4]). The second one is given by the double differential cross section in eq. (6.3) via integrations over T_1 and U_1, where the boundaries of T_1 and U_1 are given by the hadronic analogues of the partonic ones in eq. (5.1). Both computations have to yield the same result. This we checked in the following way. Take a simple expression for the two-to-three body matrix element of the parton–parton process As an example we took $|M|^2 = 1, s_4^{-1}, s_4^{-1}\ln(s_4/m^2)$. First we checked analytically that both procedures to compute the hadronic cross section lead to the same result provided one takes a simple form for the parton distribution functions (e.g $f(x) = 1$ or $f(x) = x$). This serves as a check on the correctness of the boundaries Moreover we also compared the analytic result with the numerical one and we found agreement within less than 1%, which seems to us sufficient for phenomenological purposes. Further we could also compare the analytically calculated distributions for the simple examples given above with the numerical ones and perfect agreement was obtained Finally we checked that if the physical distributions presented in the subsequent part of this section are integrated over the whole phase space they agree with the total hadronic cross section determined by the first method For our numerical results we expressed the hadronic differential cross sections as convolutions of the parton–parton differential cross sections with the parton flux functions, cf ref [4]. Then the order of the integrations was inverted to leave the p_t and/or the y integration to the last The three-dimensional integral for the S + V piece was always converted into a four-dimensional integral so that it could be directly added to the four-dimensional integral for the hard part, and the sum computed by Monte Carlo In that way we could easily project out all physically relevant distributions Detailed discussions and formalisms for calculating various distributions will be presented in appendix C.

In this section we are particularly interested in those hadronic reactions where the pair (H_1H_2) stands either for $(p,\bar{p})$ or (p,p) with p and $\bar{p}$ denoting the proton and antiproton respectively At the end of the section we will, however give some results for pion–nucleon collisions

In our previous paper [9] we examined the exact results for total hadronic cross sections and compared them with simple approximate formulae, namely initial-state gluon bremsstrahlung (ISGB), gluon splitting (GS) and flavour excitation (FE) The analytic results for these approximations were presented in sect 2 of ref [9], some of them are used in present Monte Carlo simulations of heavy flavour production. We found that the basic mechanisms mentioned above yielded values for the hadronic cross sections which were too large since they did not incorporate correctly the structure found in the parton–parton cross section However we were able to add appropriate fudge factors which made the results acceptable Now that we have calculated all the order $\alpha_s^3(Q^2)$ corrections to the differential distributions we can examine the agreement between the exact p_t, y plots and those derived from the approximate formula mentioned above In all cases we incorporate in the approximate formulae the fudge factors explained in sect. 4 of ref. [9].

We remind the reader that although the parton distribution functions and the reduced parton cross sections in eq (6.7) have to be determined in the same scheme (e.g $\overline{\mathrm{MS}}$ or DIS), the hadron–hadron cross sections still depend on the chosen factorization scale Q^2 This is because the parton distribution functions are resummed in all orders of perturbation theory via the renormalization group equation whereas the corrections to the parton–parton cross sections are only calculated to first order in $\alpha_S(Q^2)$. Since the lowest order cross section for heavy flavour production is already of order $\alpha_S^2(Q^2)$, the order $\alpha_S(Q^2)$ corrected result will heavily depend on the choice of the factorization (renormalization) scale. This phenomenon is characteristic for all pure QCD cross sections To make a comparison with the results of [2,3,28] we choose the renormalization scheme for the running coupling constant where all the heavy fermions are decoupled in the limit when the momenta entering the fermion loop contribution go to zero, cf. eq (2 15) The results for the reduced parton–parton cross sections presented in sect 5 were calculated in both the $\overline{\mathrm{MS}}$ and DIS schemes (where in the latter the momentum sum rule has been imposed, which only affects the gluon–gluon and gluon–(anti)quark partonic cross sections but not the quark–antiquark one) Since the structure functions in the latter scheme are known we will now concentrate on differential distributions for reaction (6 1) in the DIS scheme.

To be specific we will use set 2 of the DFLM [26] structure functions and the two-loop corrected formula for the running coupling constant $\alpha_S(Q^2)$ (see eq (10) in ref. [27] or eq. (54) in ref [9]) with $\Lambda_4 = 260$ MeV and $\Lambda_5 = 173$ MeV to generate the curves presented in this section. The factorization scale (which equals the renormalization scale μ_R^2) is chosen to be $Q^2 = m^2 + p_t^2$ unless stated otherwise. Further like in ref [3] we take the average of the heavy quark and the heavy antiquark differential cross sections since the difference between them is small for hadron–hadron colliders at large c.m energies

First of all to check that our results agree with those in ref [3] we present some results for the production of top quarks in $\mathrm{p\bar{p}}$ collisions for the same value of the t mass, namely 40 GeV/c^2, chosen in that paper. This, of course, is no longer a possible value for the t quark mass since the present limits [5–7] are much larger However it is now clear that the t quark mass is so heavy that it can probably only be produced near threshold at the Fermilab tevatron (if its mass is in the appropriate range). Hence results near threshold are especially important and the situation when the t mass has a value of 40 GeV/c^2 at the CERN $\mathrm{Sp\bar{p}S}$ is therefore typical.

The contributions of the gluon–gluon sub-process to the double differential cross section for eq (6.1) in p_t and y with $m = m_t = 40$ GeV/c^2 and $\sqrt{S} = 630$ GeV are shown in fig 8 Here we plot curves for both our exact and approximate calculations at two different rapidity values $y = 0$ and $y = 1\,1$. Notice that the small difference between our exact results and those of ref. [3] (fig 6) in the low p_t region, are either caused simply by numerical problems, or possibly by the imposition of the momentum sum rule in defining the gluon structure functions. If we switch off the terms (B.7) and (B.8) in appendix B then we get exact agreement

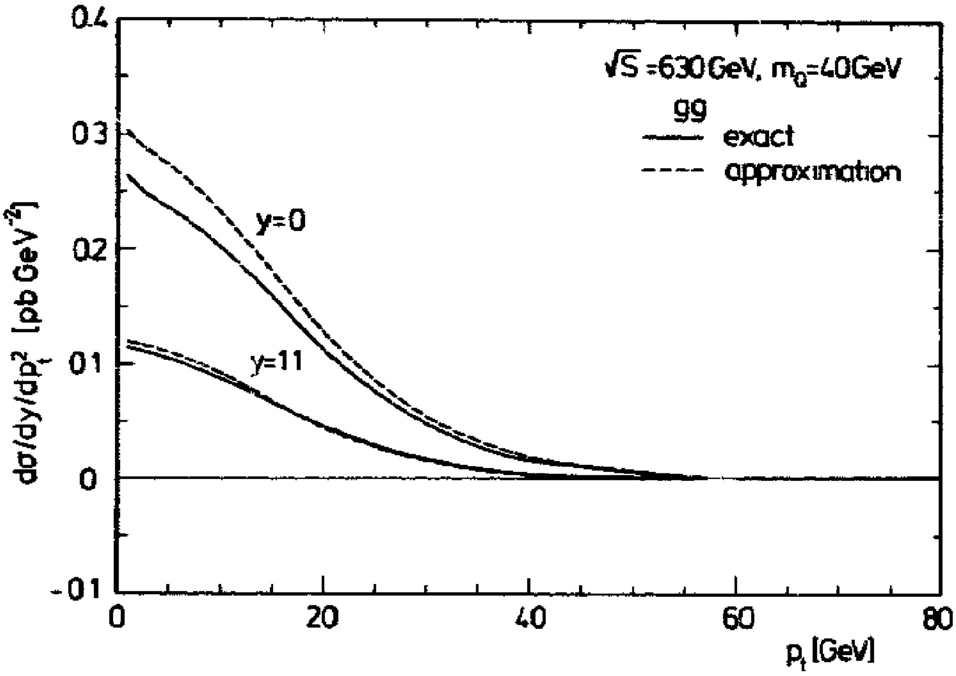

Fig 8 The contributions from the gluon–gluon sub-process to the differential cross section for $p + \bar{p} \to \bar{Q} + X$ at two different rapidity values $y = 0$ and $y = 1$ 1 Our exact results are shown for $\sqrt{S} = 630$ GeV with $m_Q = 40$ GeV$/c^2$ and $\Lambda_5 = 173$ MeV We choose the renormalization scale equal to the factorization scale $\mu_R = Q = \sqrt{m_Q^2 + p_t^2}$ We also show the results of our approximate calculations

with their curves. The dashed curve for the approximate result is 10% too large for small p_t at $y = 0$ However it is an excellent fit at $y = 1$ 1.

The corresponding curves for the quark–antiquark process are shown in fig 9. Here there is excellent agreement with the corresponding exact results in fig. 6 in ref [3] The dashed lines for the approximations are very reasonable in this channel. Finally in fig 10 we show the contribution from the gluon–antiquark channel which is the smallest of the three The approximate result is uniformly positive since our approximation is based on a cross section estimate Hence it cannot account for the negative piece of the gluon–antiquark cross section visible in fig. 6 of this paper. Since this channel only contributes a very small term to the total distribution this is acceptable

We now turn to the production of b($\bar{b}$) quarks In figs 11, 12 and 13 we show the inclusive differential cross sections in p_t for values of $y = 0$ and $y = 2$ for the channels gg, $q\bar{q}$ and $g\bar{q}$. We have chosen $m_b = 4$ 75 GeV$/c^2$ and $\sqrt{S} = 630$ GeV In the gluon–gluon and quark–antiquark channels the approximate results are excellent for small p_t but are too large by as much as a factor of two at $y = 0$ and $p_t = 80$ GeV$/c$ This is caused by the fact that the exact order α_S correction is negative at these large p_t values so the Born value is reduced and our positive approximation goes in the wrong direction In the gluon–antiquark channel the approximate results shown in fig. 13 are too small below $p_t = 15$ GeV$/c$ and too

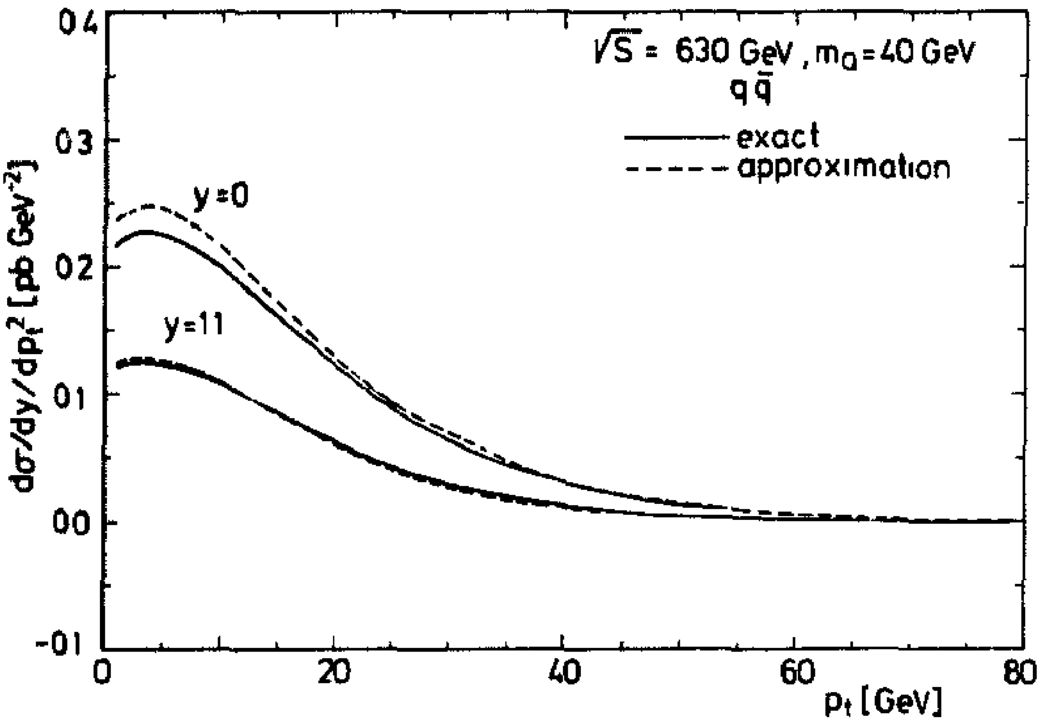

Fig 9 The same as in fig 8, but for the quark–antiquark sub-process

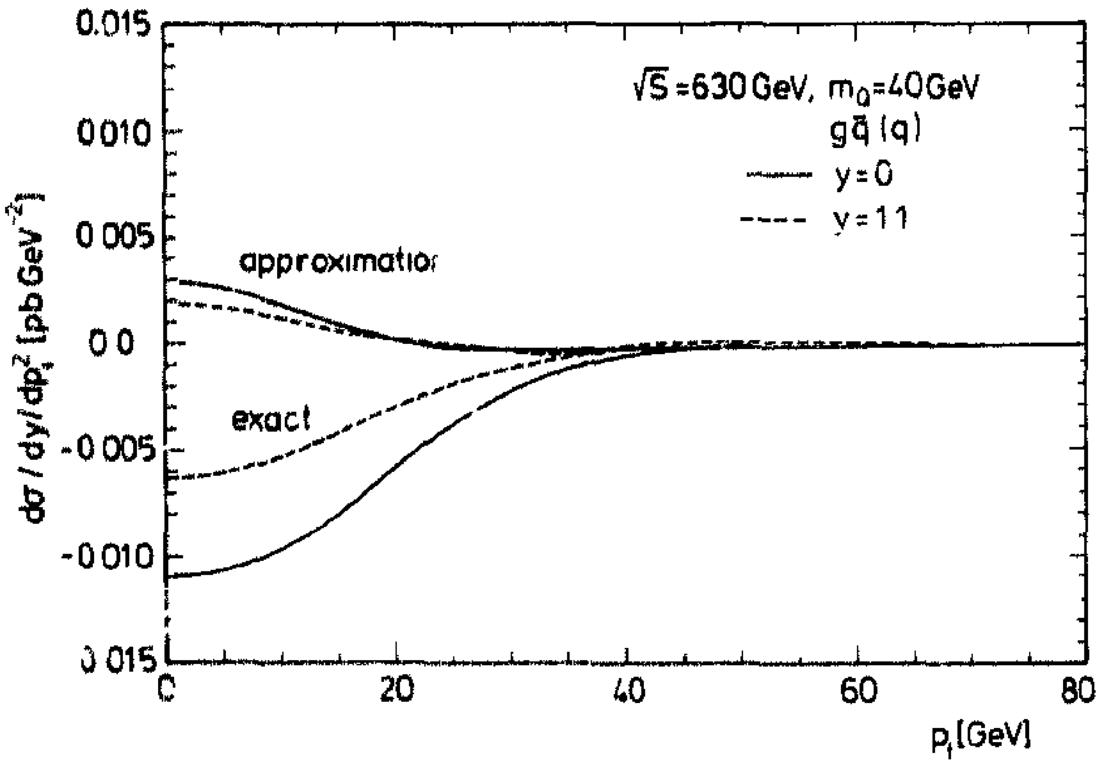

Fig. 10 The same as in fig 8, but the gluon-(anti)quark sub process Here the two lower curves refer to our exact calculations and the upper ones to our approximations

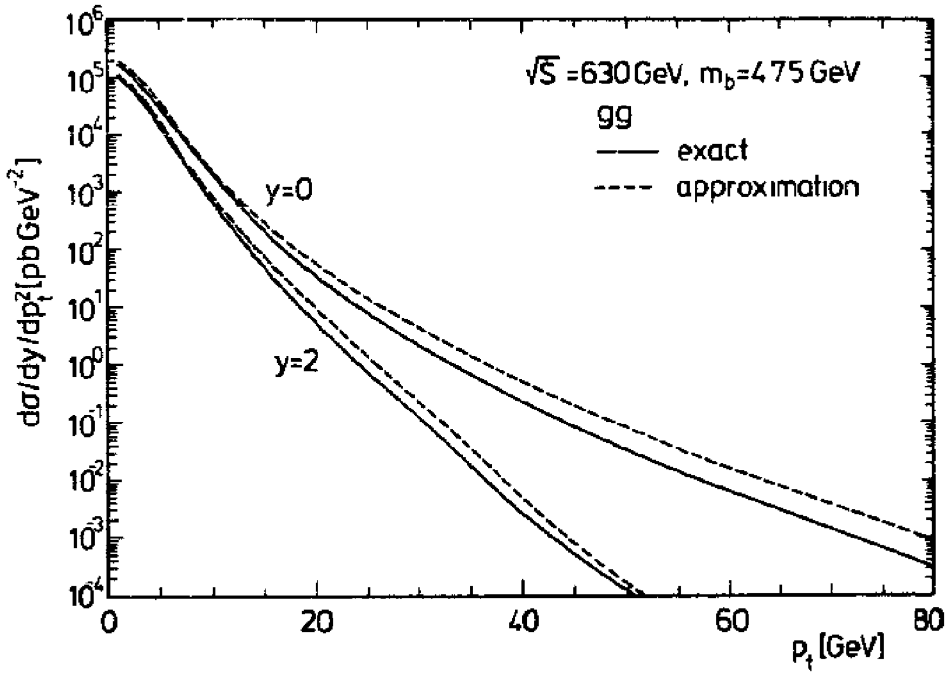

Fig 11 The same as in fig 8, but for $m_b = 4.75$ GeV/c^2, $\sqrt{S} = 630$ GeV, $\Lambda_4 = 260$ MeV and $y = 0, 2$

large above that value Below $p_t \sim 5$ GeV/c the approximate results deviate substantially from the exact ones since the approximations do not account for the negative piece of the gluon–antiquark cross section.

Next we present in fig. 14 the total α_S^3 differential cross sections in p_t for values of $y = 0$, 2 and 3 We have chosen $m_b = 4.75$ GeV/c^2 and $\sqrt{S} = 630$ GeV. The curves at $\sqrt{S} = 1.8$ TeV, for $y = 0$, 3 and 4 are shown in fig. 15. Note that we have checked that our results agree with the corresponding curves in figs. 11 and 12 of ref [3] which are unfortunately labelled incorrectly The b-quark mass is given as $m_b = 5$ GeV/c^2 whereas it should have been listed as $m_b = 4.75$ GeV/c^2

The rapidity plots of the outgoing b quark are shown in fig 16 separately for the order α_S^2 and order α_S^3 contributions at the energies $\sqrt{S} = 630$ GeV and $\sqrt{S} = 1.8$ TeV. Again to cross check our results with those of ref [3] we give a plot of their fig. 16 in our fig. 17. This is for c quark production at $\sqrt{S} = 630$ GeV and 1.8 TeV, with a mass $m_c = 1.5$ GeV/c^2 and scale $Q^2 = 4(p_t^2 + m^2)$. It is clear that the Born result in ref [3] for $\sqrt{S} = 1.8$ TeV is too low near $y = 0$. Our other curves agree with theirs We remind the reader that results for the production of charmed quarks are very sensitive to the choice of the scale factor Q^2 and the mass of the c quark.

Next we present in fig. 18 the sum of all contributions, namely the inclusive cross section for the production of a bottom quark with $p_t > p_{min}$ and a fixed rapidity cut $|y| < 1.5$ at $\sqrt{S} = 630$ GeV. In this plot the scale $Q^2 = m_b^2 + p_{min}^2$ has been used in the definition of the running coupling constant. We have chosen a central value of

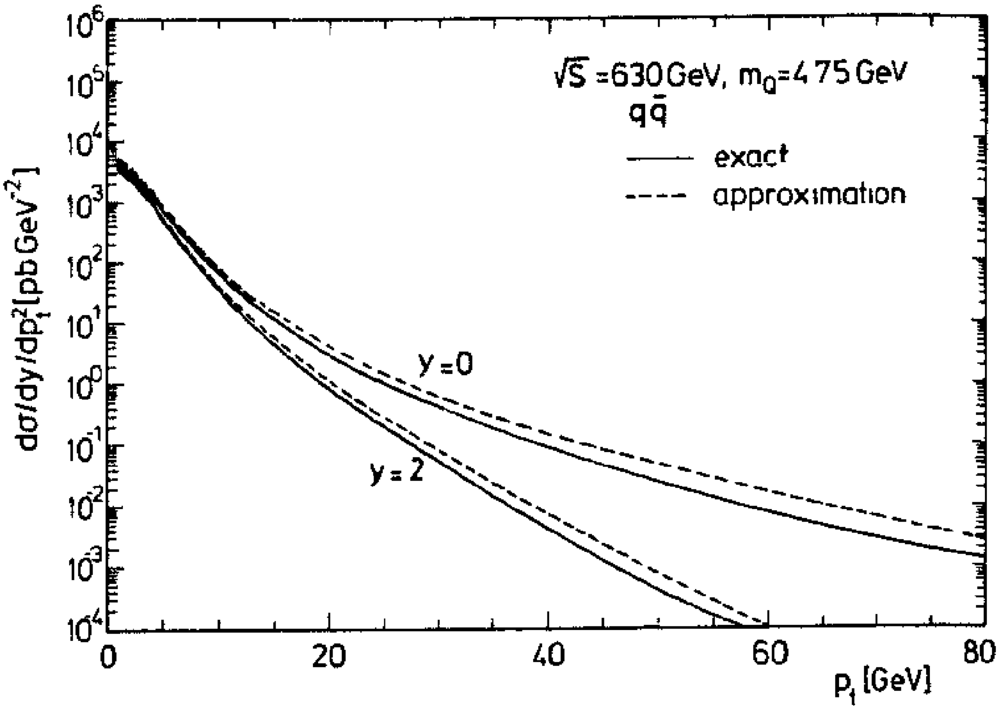

Fig 12 The same as in fig 11, but the quark–antiquark sub-process

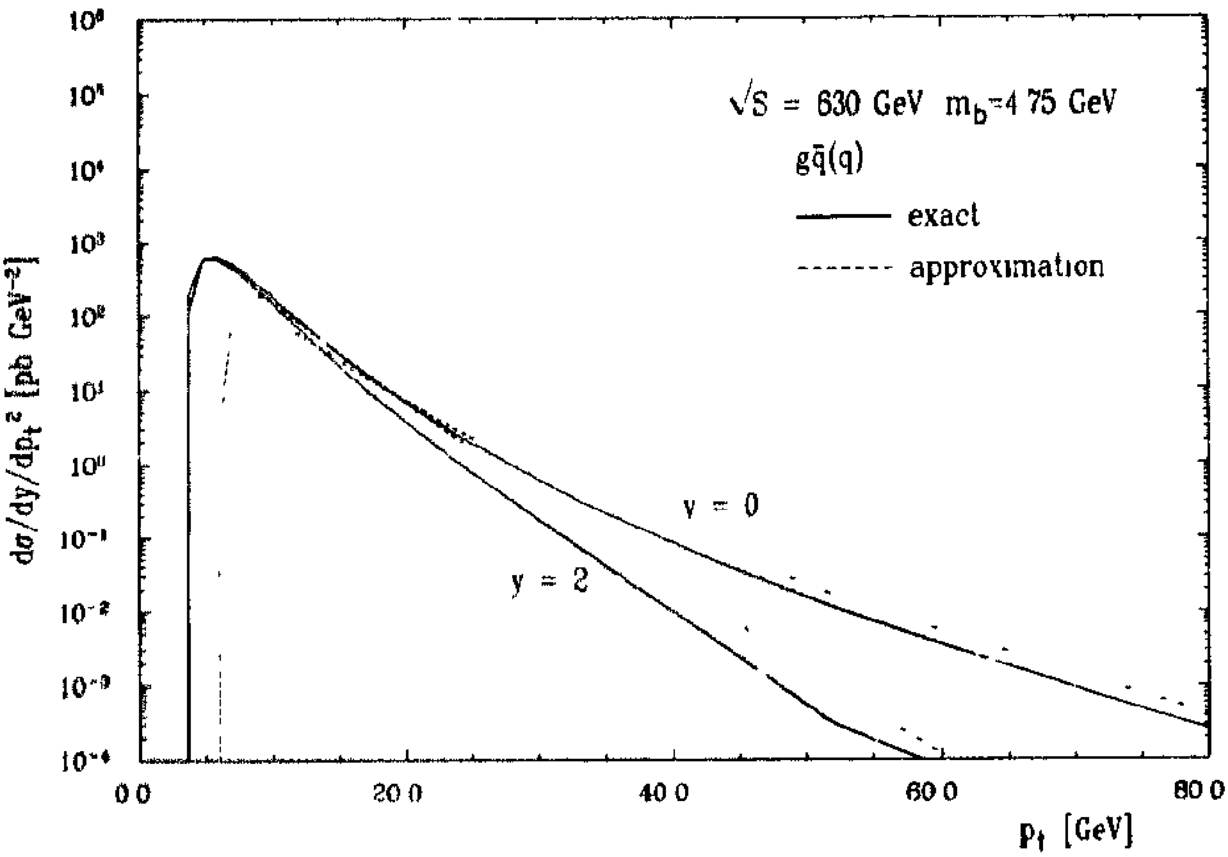

Fig. 13 The same as in fig 11, but for the gluon–(anti)quark sub-process

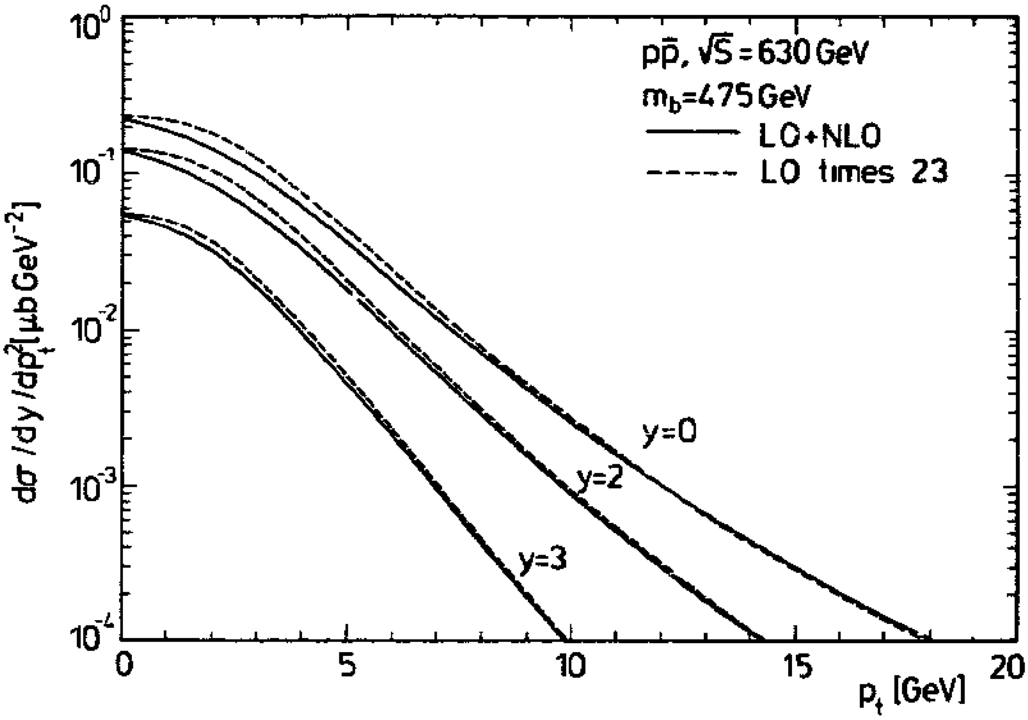

Fig 14 The differential cross section of $p + \bar{p} \to b + X$ with $m_b = 4.75$ GeV/c^2 and $\mu_R = Q = \sqrt{m_b^2 + p_t^2}$ at $\sqrt{S} = 630$ GeV The cross section is shown at different values of rapidity for (1) dashed lines lowest order contribution scaled by an arbitrary factor (2) solid lines full order α_S^3 calculation

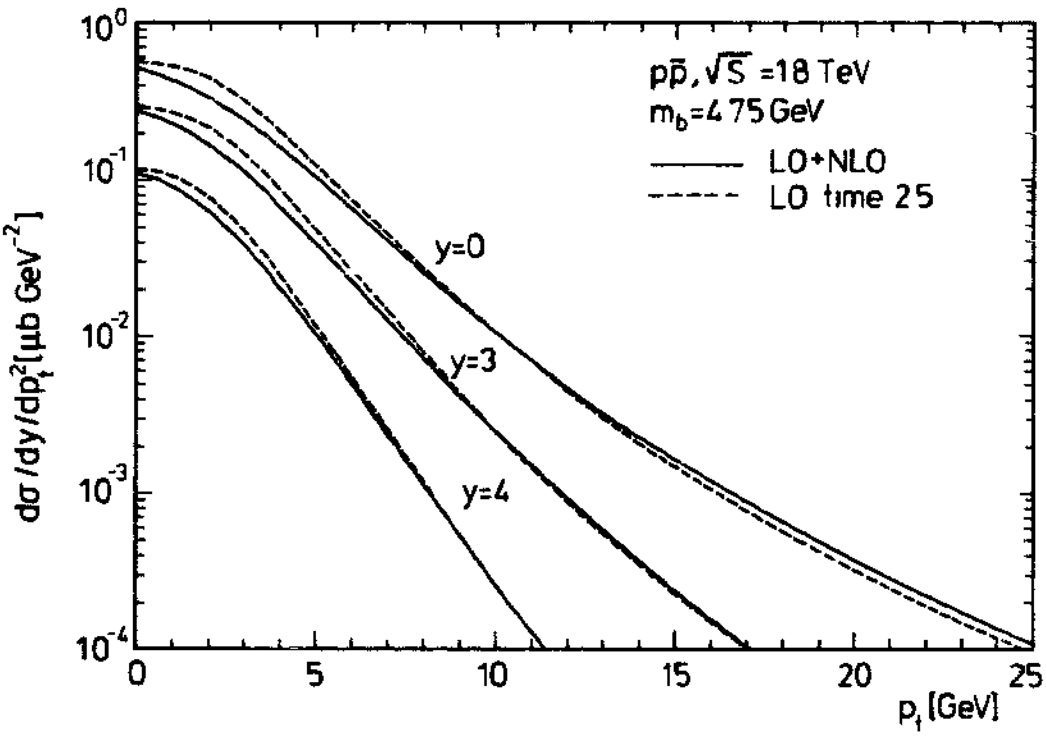

Fig 15 The same as in fig 14 but with $\sqrt{S} = 1.8$ TeV

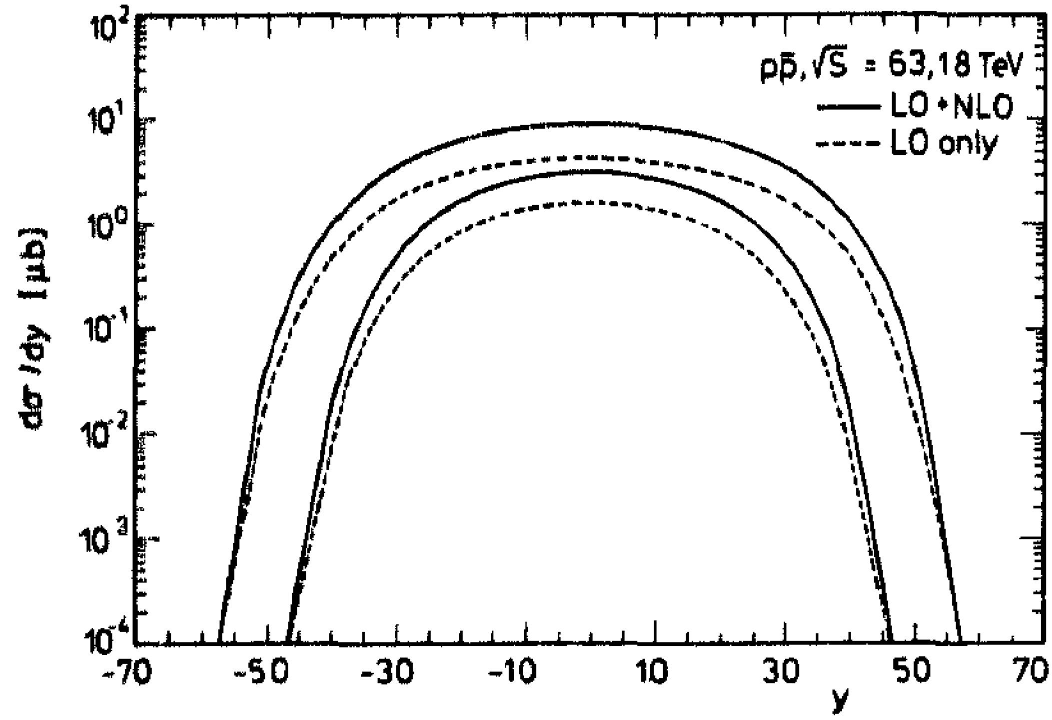

Fig. 16. The rapidity distribution for $p + \bar{p} \to b + X$ with $m_b = 4.75$ GeV/c^2, $\mu_R = Q = \sqrt{m_b^2 + p_T^2}$ at $\sqrt{S} = 630$ GeV and $\sqrt{S} = 1.8$ TeV. The upper curves refer to the higher energy.

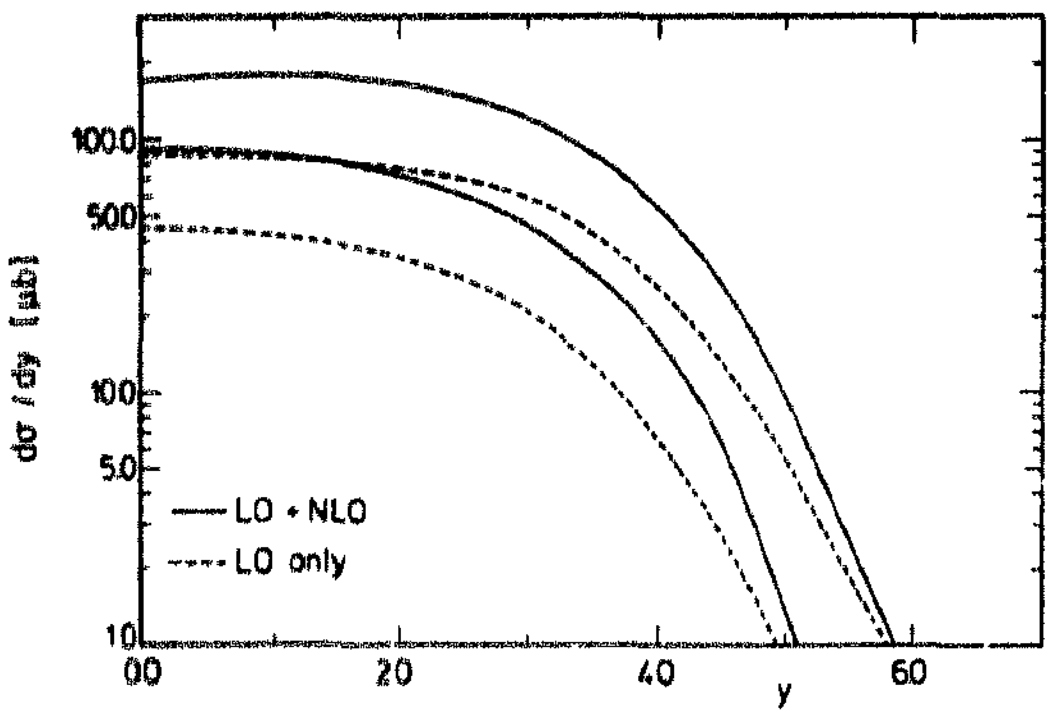

Fig. 17. The rapidity distribution of inclusive charm quark production in $p\bar{p}$ collisions at $\sqrt{S} = 630$ GeV and $\sqrt{S} = 1.8$ TeV. The charm quark mass is taken as $m_c = 1.5$ GeV/c^2, $\mu_R = Q = 2\sqrt{m_c^2 + p_T^2}$ and $\Lambda_4 = 260$ MeV.

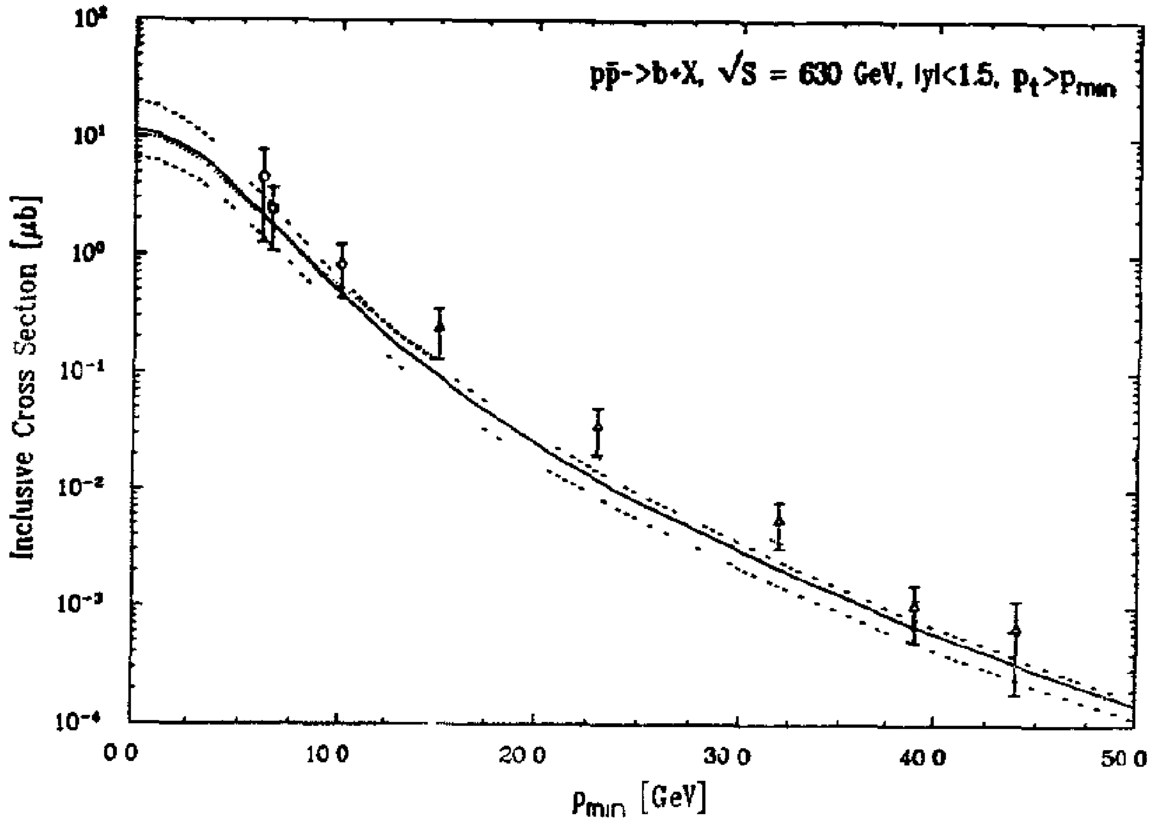

Fig 18 The inclusive cross section for b and/or $\bar{b}$ quark production at $\sqrt{S} = 630$ GeV versus $p_{\min}$ with $m_b = 4\ 75$ GeV$/c^2$, $\mu_R = Q = \mu_0 = \sqrt{m_b^2 + p_{\min}^2}$, DFLM set 2 with $\Lambda_4 = 260$ MeV and fixed rapidity cut $|y| < 1\ 5$ (solid line exact result, dotted line result of our approximate calculation) The upper (lower) dashed line is obtained from the exact order α_S^3 calculation by using $m_b = 4\ 5\ (5\ 0)$ GeV$/c^2$, $\mu_R = Q = \mu_0/2\ (2\mu_0)$ and DFLM set 3 (1) with $\Lambda_4 = 360\ (160)$ MeV The re-analyzed UA1 data are also shown

the b-quark mass as 4 75 GeV$/c^2$. The band bounded by the two dashed lines in fig. 18 is generated by choosing 4.5 GeV$/c^2 < m_b < 5\ 0$ GeV$/c^2$, 360 MeV $> \Lambda_4 >$ 160 MeV, $(m_b^2 + p_{\min}^2)/4 < Q^2 < 4(m_b^2 + p_{\min}^2)$ and DFLM set 3 and DFLM set 1 In this plot we show the re-analysed data from the UA1 group [28]. It is clear that there is very reasonable agreement between theory and experiment

We also plot in this figure (dotted line) the sum of our approximate formulae as presented in ref. [9]. One sees that our approximate result in fig. 18 is in good agreement with the exact curve at small p_t but is about a factor of two larger than our exact result at $p_{\min} = 50$ GeV$/c$ To better understand the origin of this discrepancy we plot in fig. 19 the individual contributions from the ISGB, GS and FE mechanisms to the transverse momentum distribution for the production of a b quark with $m_b = 4\ 75$ GeV$/c^2$ at $\sqrt{S} = 630$ GeV. We see that the sum of the Born and the ISGB part is fine at small p_t where the contributions from the GS and FE mechanisms are small. The ISGB part is, however, too big at larger p_t where the GS and FE mechanisms are also important. The total contribution from the

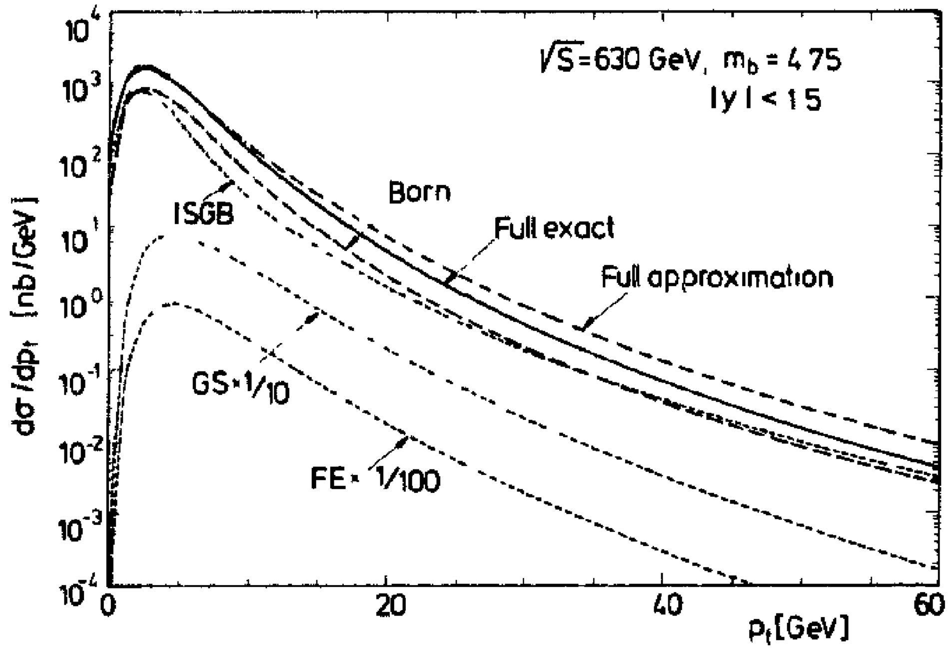

Fig. 19. The transverse momentum distribution for the production of b quarks $p + \bar{p} \to b + X$, with $m_b = 4.75$ GeV/c^2, $\mu_R = Q = \sqrt{m_b^2 + p_t^2}$ at $\sqrt{S} = 630$ GeV. The contributions from ISGB, GS and FE are shown separately.

approximation is about a factor of two too large at p_t 50 GeV/c as compared to our exact result. Note that due to our choice of $Q^2 = p_t^2 + m_b^2$ all approximate results contain contributions from the scale-dependent pieces of the α_s^3 correction, which have also been multiplied by the appropriate fudge factors discussed in ref [9]. Given the present experimental error bars one can conclude that a very reasonable fit to the data is to take the sum of all approximate contributions for $p_t < 10$ GeV/c, but only those of the Born cross section plus the GS and FE contributions above $p_t = 10$ GeV/c.

In fig. 20 we show predictions for b-quark production at the Fermilab collider. The parameters are the same as in fig. 18, but we have changed the rapidity cut to $-1.0 < y < 1.0$ as appropriate for the CDF detector. Notice that our error band is not exactly the same as in fig. 15 of ref. [3] since we do not add up various uncertainties in quadrature as they did in their calculation. It will be interesting to see whether these predictions fit the future CDF data.

Since one would like to understand whether the α_s corrections are describable by a simple K-factor we have plotted in fig. 21 the p_t distribution for a heavy t-quark with a mass of 120 GeV/c^2 produced in $p\bar{p}$ collisions at $\sqrt{S} = 1.8$ TeV. In this situation a K factor of 1.4 is reasonable at large p_t and y values. However it overestimates the curves for small p_t and y. We finalize this discussion of heavy quark production at colliders by giving a plot of top quark cross sections for tevatron and future colliders in fig. 22.

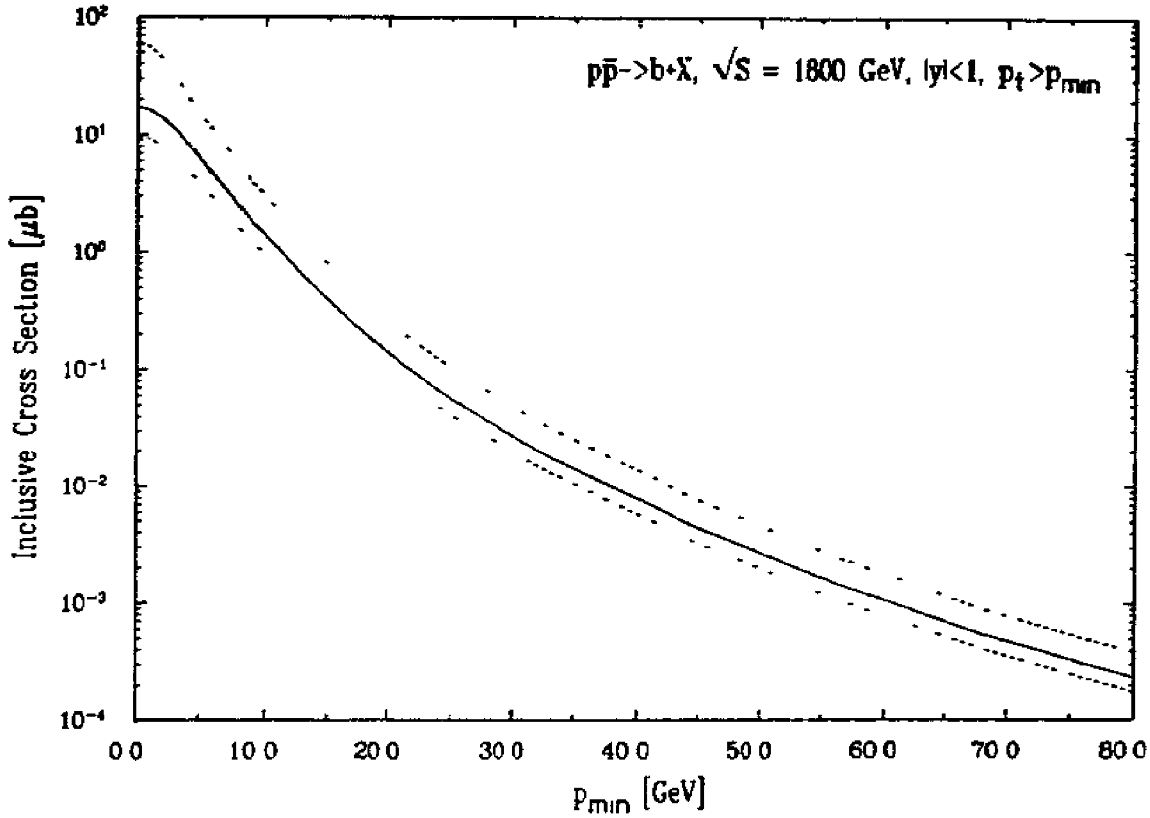

Fig 20 The same as in fig 18, but for $\sqrt{S} = 1.8$ TeV and $|y| < 1$

We now turn to a short discussion of differential distributions for the production of c and b quarks in fixed target experiments This is a situation where the total c.m. energies are small and the theoretical results are very sensitive to the choice of the mass and the scales. A more complete discussion of these points is given in ref [?] The reason we present our results here is to correct several of the plots in the latter paper. We have checked that we agree with the plots for the total cross sections in figs. 22 and 23 of ref. [3]. Also the plots for the p_t distributions in figs. 19 and 26 agree with our results We disagree, however, with the plots for the $x_F = p_L/p_{L,max}$ distributions. One can check the areas under the curves in figs. 18 and 25 of ref [3] are not the same as the areas under the curves in figs. 19 and 26 of ref [3], respectively. In fig. 23 we show the x_F distribution for charm production in pp collisions at c.m. energies of 27.4, 38.7 and 62 GeV Here $m_c = 1.5$ GeV/c^2, the scale is $Q^2 = 4(p_t^2 + m_c^2)$, and we have chosen the DFLM structure functions set 2 with $\Lambda_4 = 260$ MeV. The corresponding results from ref. [3] are in their fig. 18. The x_F plots for $\pi^- p$ collisions at $\sqrt{S} = 23$ GeV are shown in fig. 24. In this case we have used set 1 of the pion structure functions of Owens in ref. [29] Unfortunately the corresponding structure functions used by ref. [3] contained an error leading to incorrect curves in their fig. 21. This same error also changes their plots of the x_F distributions for b-quark production in $\pi^- N$ collisions at $\sqrt{S} = 23$

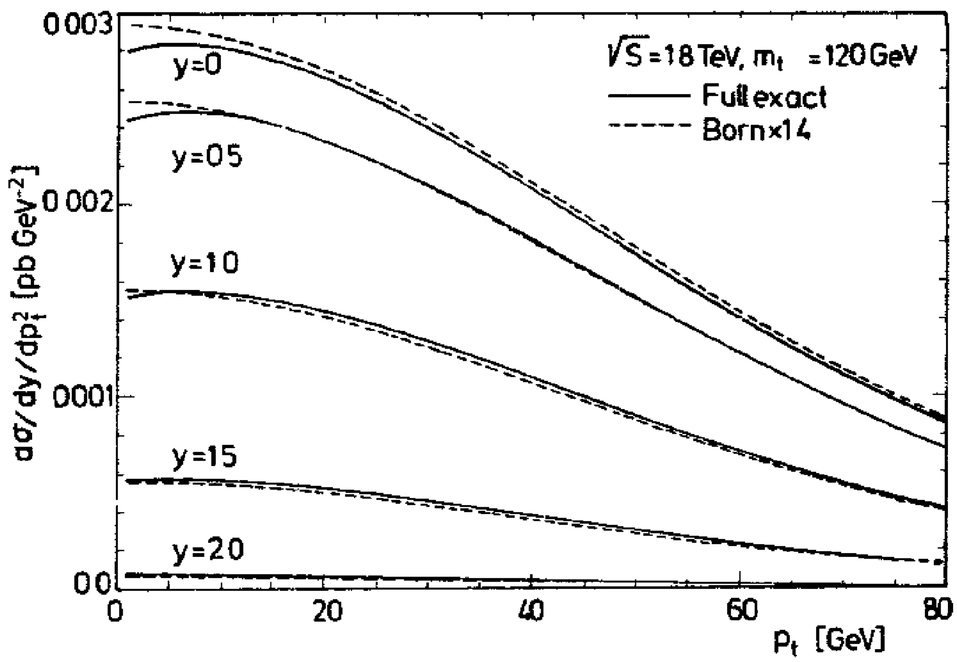

Fig 21 The differential cross section for $p+\bar{p} \to t(\bar{t})+X$ with $m_t = 120$ GeV/c^2 and $\mu_R = Q = \sqrt{m_t^2+p_t^2}$ at $\sqrt{S} = 1.8$ TeV The cross section is shown at different values of rapidity for (1) dashed lines lowest order contribution scaled by an arbitrary factor (2) solid lines full order α_s^3 calculation

GeV and $\sqrt{S} = 30$ GeV, given in fig. 24 of their paper The correct distributions are presented in our fig 25 The final curves we present in fig 26 are those for b quark production in pN collisions at $\sqrt{S} = 46$ GeV and in pp collisions at $\sqrt{S} = 62$ GeV. This figure corresponds to fig 25 of ref [3] which also seems to contain errors. To check that our results are the correct ones we have also computed the cross sections from the parton–parton cross sections and they agree with the cross sections from the x_t plots

We conclude our discussion of the heavy quark differential cross sections in hadron–hadron collisions with the following comments The comparison with the UA1 data on b-quark production, cf fig 18, shows the necessity of taking higher order corrections into account. Even though there is still a small uncertainty in the choice of the b-quark mass and the scale for α_s, perturbative QCD seems to describe b-quark production rather well The differential cross section is not very sensitive to the choice of the gluon structure functions since the $q\bar{q}$, gq and $g\bar{q}$ channels are all important at large p_t. Note that we have only used the structure functions provided by DFLM in fig 18 because the parton–parton cross sections were calculated in a modified DIS scheme

The approximate formulae for the differential cross sections given in sect. 2 of ref. [9] with the fudge factors mentioned there lead to very reasonable distributions in p_t at low p_t where the ISGB mechanism is dominant. However they are uniformly too big at larger p_t where the contributions from the GS and FE

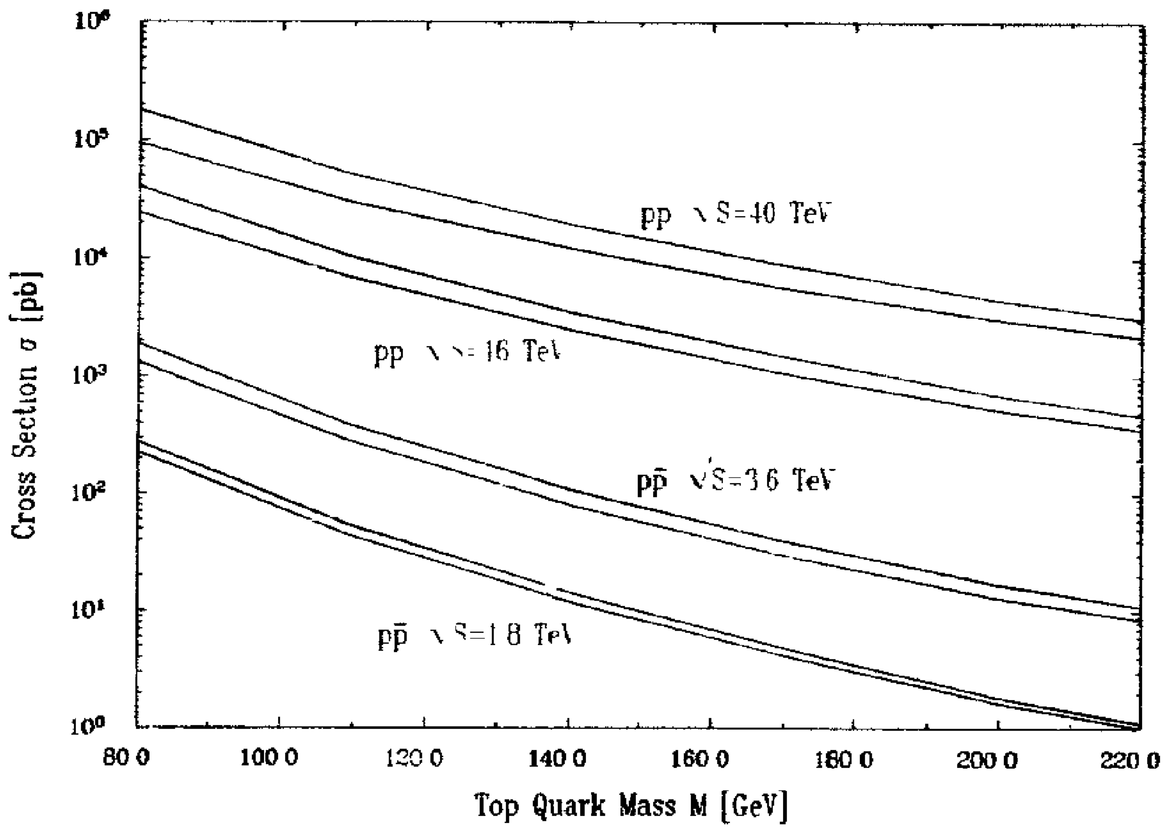

Fig 22 Predicted top quark total cross sections at Fermilab $p\bar{p}$ collider with energy $\sqrt{S} = 1\ 8$ TeV, an upgraded Fermilab $p\bar{p}$ collider with energy $\sqrt{S} = 3\ 6$ TeV an LHC pp collider with energy $\sqrt{S} = 16$ TeV and an SSC pp collider with energy $\sqrt{S} = 40$ TeV The bands are indications of theoretical uncertainties which are obtained by using $\mu_R = Q = m_t/2$ DFLM set 3 with $\Lambda_5 = 250$ MeV and $\mu_R = Q = 2m_t$, DFLM set 1 with $\Lambda_5 = 101$ MeV

channels are relatively more important This result is consistent with the p_t distribution for b-production originally shown in the UA1 fit of their data [8] since they only included the Born, GS and FE in their analysis The slope of their prediction for the p_t distribution was therefore smaller than that from the exact calculation, since it lacked the ISGB piece necessary to fit the data at low p_t

One motivation for this paper was to find if a simple K-factor could be found to account for the higher order corrections. However the total and single-particle inclusive differential cross sections for heavy-quark production show such complicated behaviour that this approach has not been as successful as we had originally hoped. The structure in the parton–parton cross sections seen in the results of [2, 4, 9] are reflections of integrations over equally complicated structures in the parton–parton differential cross sections

We would like to acknowledge useful discussions with A. Ali, G Ingelman, G Kramer, D E Soper and J. Vermaseren R. Meng would like to thank LAA for

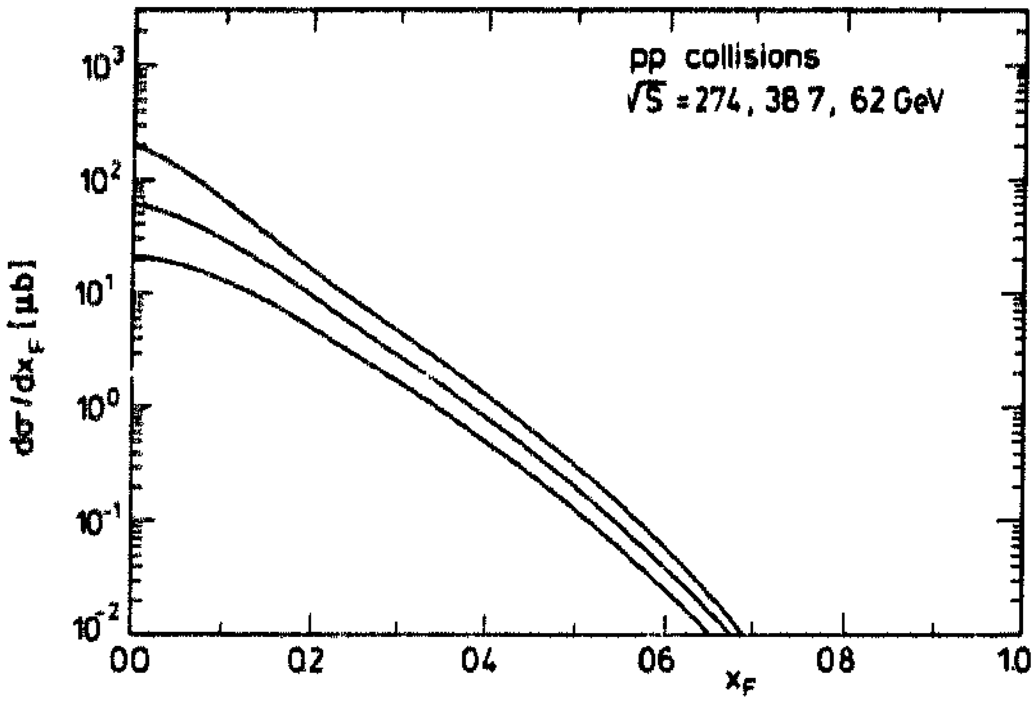

Fig. 23. The x_F distribution of inclusive charm quark production in pp collisions at c.m. energies 27.4, 38.7 and 62 GeV. The parameters are $m_c = 1.5$ GeV/c^2, $\Lambda_4 = 260$ MeV and $\mu_R = Q = 2\sqrt{m_c^2 + p_T^2}$. The upper curves refer to higher energies.

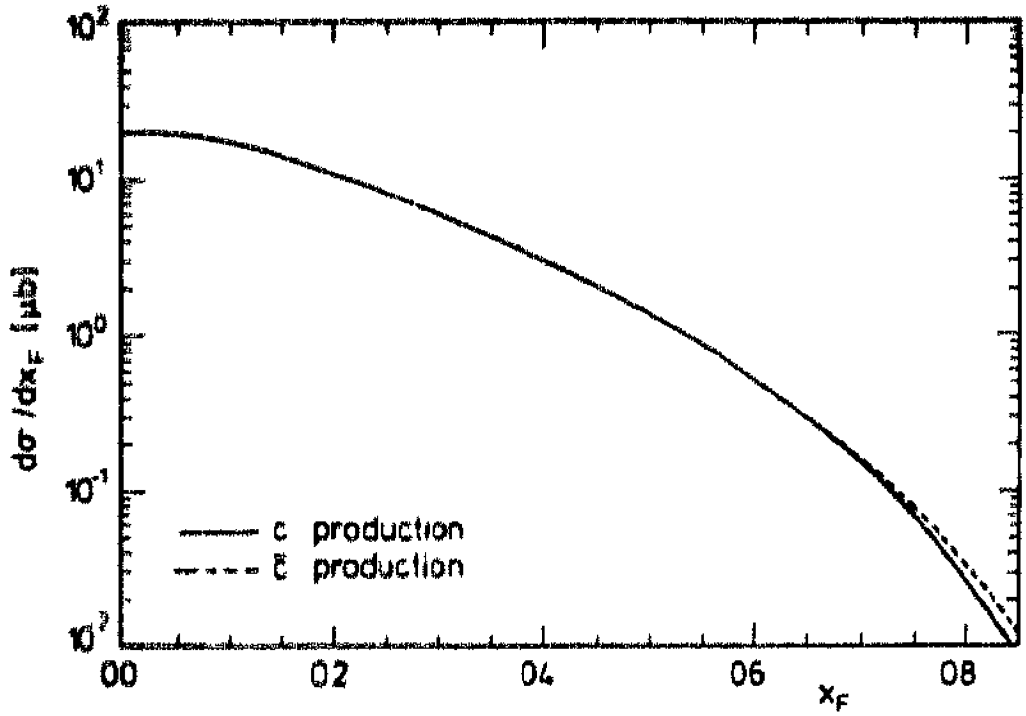

Fig. 24. The x_F distribution of c (solid line) and $\bar{c}$ (dashed line) production in π^-p collisions at a c.m. energy of 23 GeV. The parameters are $m_c = 1.5$ GeV/c^2, $\Lambda_4 = 260$ MeV, $\mu_R = Q = 2\sqrt{m_c^2 + p_T^2}$, DFLM set 2 for the proton structure functions and set 1 of ref. [29] for the pion structure functions.

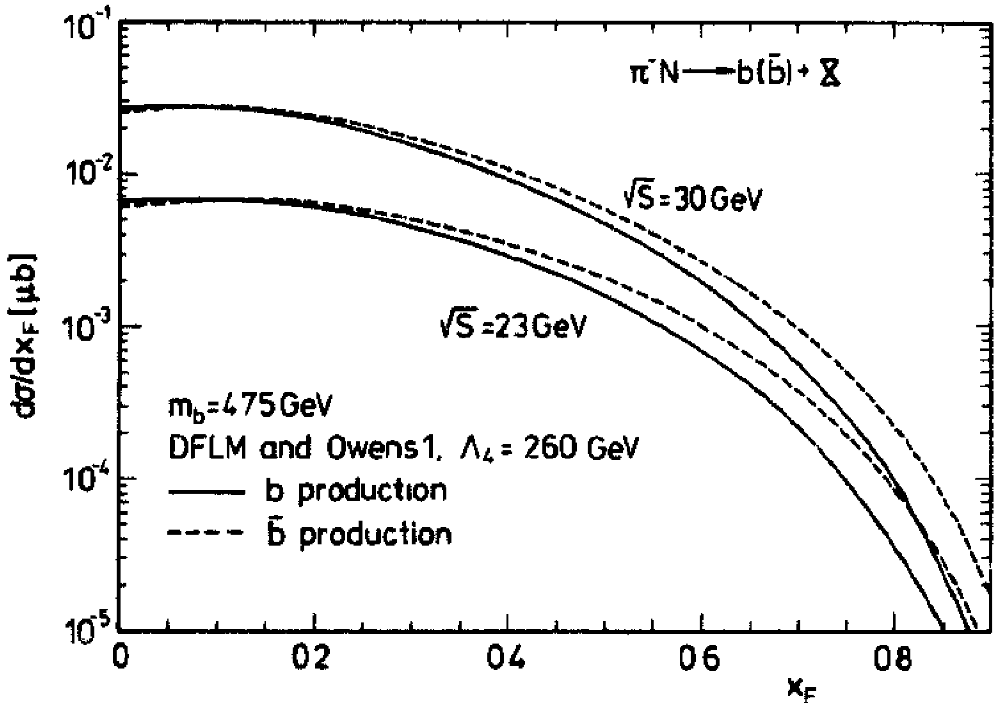

Fig 25. The x_F distribution of b (solid line) and $\bar{b}$ (dashed line) production in $\pi^- N$ collisions at c m energies of 23 and 30 GeV The parameters are as in fig 24 but $m_b = 4.75$ GeV/c^2 and $\mu_R = Q = \sqrt{m_b^2 + p_t^2}$

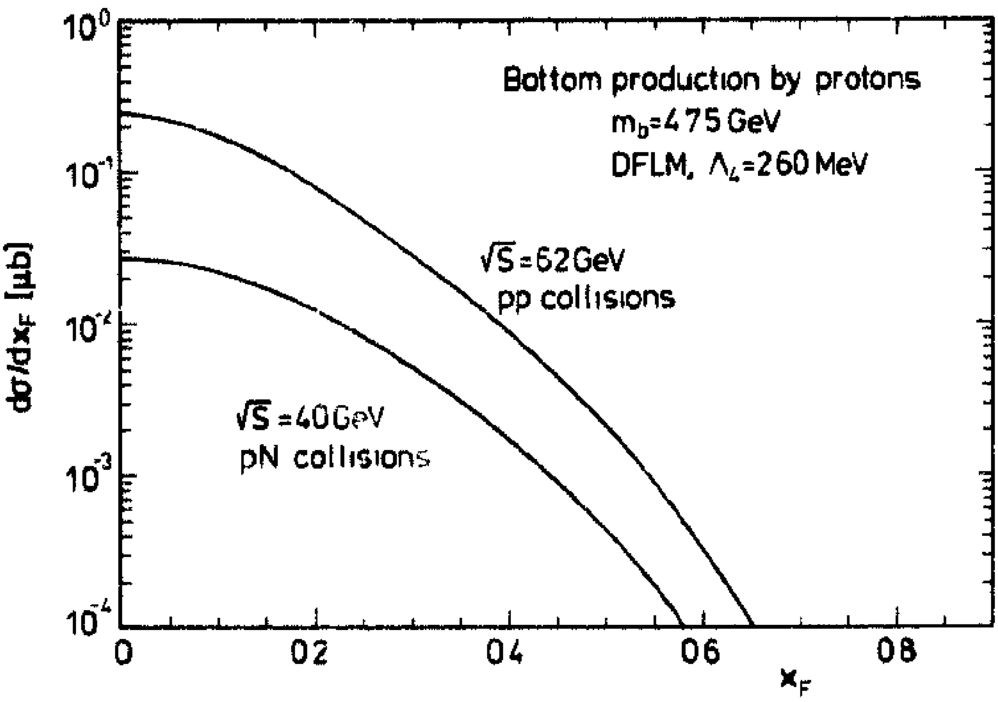

Fig. 26. The x_F distribution of inclusive bottom quark production in pN collisions at c.m energy of 40 GeV and pp collisions at 62 GeV. The parameters are $m_b = 4.75$ GeV/c^2, $\mu_R = Q = \sqrt{m_b^2 + p_t^2}$ and DFLM set 2 with $\Lambda_4 = 260$ MeV.

financial support. The work of J. Smith was supported in part under NSF Grant PHY 89-089495 and in part by NIKHEF-H in Amsterdam.

Appendix A

In this appendix we give the results for the virtual plus soft parton cross sections in eq. (4.7). The cross sections can be split in symmetric and antisymmetric parts as follows. The F part is equal to

$$
\begin{aligned}
\left(s^2 \frac{\mathrm{d}^2\hat{\sigma}^{(1)}_{q\bar{q},\mathrm{F}}}{\mathrm{d}t_1\,\mathrm{d}u_1} \right)^{\mathrm{V+S}}_{\overline{\mathrm{MS}}}
&= \tfrac{1}{4}\alpha_s^3(\mu_R^2) K_{q\bar{q}} N C_F^2 \Bigg[A_{\mathrm{QED}} \Bigg\{ 8\ln^2\delta - 8\ln\delta \Bigg(\ln\frac{t_1u_1}{sm^2} + 1 \\
&\quad + (s-2m^2)\bar{s}^{-1}\ln x \Bigg) + \ln\frac{Q^2}{m^2}\left(-8\ln\delta + 4\ln\frac{t_1u_1}{m^4} - 6 \right) \\
&\quad + 4(s-2m^2)\bar{s}^{-1}\big(-3\ln x - \tfrac{1}{2}\ln^2 x + 4\ln x\ln(1-x) \\
&\quad + 2\ln x\ln(1+x) + 4\,\mathrm{Li}_2(x) + 2\,\mathrm{Li}_2(-x) + 3\zeta(2) \big) \\
&\quad + 2s\bar{s}^{-1}\ln x + 6\ln\frac{s}{m^2} - 4\ln\frac{t_1u_1}{m^4}\ln\frac{s}{m^2} + 2\ln^2\frac{t_1u_1}{m^4} \\
&\quad + 4\,\mathrm{Li}_2\left(1 - \frac{m^2 s}{t_1u_1} \right) - 20 + 8\zeta(2) \Bigg\} + 8m^2\bar{s}^{-1}\ln x \Bigg]\delta(s+t_1+u_1) \\
&\quad + \tfrac{1}{4}\alpha_s^3(\mu_R^2) K_{q\bar{q}} N C_F^2 \Bigg[A_{\mathrm{QED}} \Bigg\{ 32\ln\delta\ln\frac{t_1}{u_1} - 16\ln\frac{t_1}{u_1}\ln\frac{s}{m^2} \\
&\quad - 16\ln x\ln\frac{t_1}{u_1} - 16\,\mathrm{Li}_2\left(1 - \frac{u_1}{xt_1} \right) + 16\,\mathrm{Li}_2\left(1 - \frac{t_1}{xu_1} \right) \Bigg\} \\
&\quad - 4(t_1-u_1)s^{-1}\left(\ln^2\frac{s}{m^2} + 2\zeta(2) \right) + 8(t_1-u_1)s_1^{-1}\ln\frac{s}{m^2} \\
&\quad + (8t_1u_1 - 16sm^2)s^{-1}u_1^{-1}\ln\frac{-u_1}{m^2} - (8t_1u_1 - 16sm^2)s^{-1}t_1^{-1}\ln\frac{-t_1}{m^2} \\
&\quad + 8(t_1-u_1)s^{-1}\bar{s}^{-1}s_1^{-1}(s^2 - 8sm^2 + 8m^4)\big(\zeta(2) + \tfrac{1}{2}\ln^2 x + 2\,\mathrm{Li}_2(-x) \big) \\
&\quad + (8 + 16u_1s^{-1})\left(-\ln\frac{-u_1}{m^2}\ln\frac{s}{m^2} + \ln^2\frac{-u_1}{m^2} + \mathrm{Li}_2\left(\frac{u_1}{m^2} \right) \right) \\
&\quad - (8 + 16t_1s^{-1})\left(-\ln\frac{-t_1}{m^2}\ln\frac{s}{m^2} + \ln^2\frac{-t_1}{m^2} + \mathrm{Li}_2\left(\frac{t_1}{m^2} \right) \right) \Bigg]\delta(s+t_1+u_1)\,.
\end{aligned}
\tag{A.1}
$$

Here $\alpha_S(\mu_R^2)$ denotes the renormalized coupling constant at the renormalization scale μ_R^2, which will be put equal to Q^2 in the end as mentioned in sect 6. For the A part we obtain

$$\left(s^2\frac{d^2\hat{\sigma}^{(1)}_{q\bar{q},A}}{dt_1\,du_1}\right)^{V+S}_{\overline{MS}}$$

$$= \tfrac{1}{4}\alpha_S^3(\mu_R^2)K_{q\bar{q}}NC_AC_F\Bigg[A_{QED}\Bigg\{4\ln\delta\left(\ln\frac{t_1u_1}{sm^2}+(s-2m^2)\bar{s}^{-1}\ln x\right)$$

$$+\tfrac{22}{3}\ln\frac{\mu_R^2}{m^2}+\ln^2\frac{s}{m^2}+\left(-\tfrac{16}{3}+s(s-16m^2)s_1^{-2}\right)\ln\frac{s}{m^2}-4\ln\frac{-t_1}{m^2}\ln\frac{-u_1}{m^2}$$

$$-2(s-2m^2)\bar{s}^{-1}\big(-2\ln x-\tfrac{3}{2}\ln^2 x+4\ln x\ln(1-x)$$

$$+2\ln x\ln(1+x)+4\,\mathrm{Li}_2(x)+2\,\mathrm{Li}_2(-x)+3\zeta(2)\big)$$

$$-s\bar{s}^{-1}\ln x-\ln^2 x-8m^2s_1^{-1}+2ss_1^{-2}\bar{s}^{-1}(s^2-7m^2s+24m^4)$$

$$\times\big(\zeta(2)+\tfrac{1}{2}\ln^2 x+2\,\mathrm{Li}_2(-x)\big)-2\,\mathrm{Li}_2\left(1-\frac{m^2s}{t_1u_1}\right)+\frac{170}{9}-6\zeta(2)\Bigg\}$$

$$-m^2s^{-1}\ln^2\frac{s}{m^2}+s_1^{-2}(-s^2+12sm^2+16m^4)\ln\frac{s}{m^2}$$

$$+(2sm^2-t_1u_1)s^{-1}t^{-1}\ln\frac{-t_1}{m^2}+(2sm^2-t_1u_1)s^{-1}u^{-1}\ln\frac{-u_1}{m^2}$$

$$-(1+2us^{-1})\left(-\ln\frac{-u_1}{m^2}\ln\frac{s}{m^2}+\ln^2\frac{-u_1}{m^2}+\mathrm{Li}_2\left(\frac{u}{m^2}\right)\right)$$

$$-(1+2ts^{-1})\left(-\ln\frac{-t_1}{m^2}\ln\frac{s}{m^2}+\ln^2\frac{-t_1}{m^2}+\mathrm{Li}_2\left(\frac{t}{m^2}\right)\right)$$

$$-4m^2s_1^{-2}\bar{s}^{-1}(s^2-2sm^2+16m^4)\big(\zeta(2)+\tfrac{1}{2}\ln^2 x+2\,\mathrm{Li}_2(-x)\big)$$

$$-4m^2\bar{s}^{-1}\ln x-2m^2s^{-1}\zeta(2)+8m^2s_1^{-1}\Bigg]\delta(s+t_1+u_1)$$

$$+\tfrac{1}{4}\alpha_S^3(\mu_R^2)K_{q\bar{q}}NC_AC_F\Bigg[A_{QED}\Bigg\{-12\ln\delta\ln\frac{t_1}{u_1}$$

$$+6\ln\frac{t_1}{u_1}\ln\frac{s}{m^2}+6\ln x\ln\frac{t_1}{u_1}-6\,\mathrm{Li}_2\left(1-\frac{t_1}{xu_1}\right)+6\,\mathrm{Li}_2\left(1-\frac{u_1}{xt_1}\right)\Bigg\}$$

$$+\tfrac{3}{2}(t_1-u_1)s^{-1}\left(\ln^2\frac{s}{m^2}+2\zeta(2)\right)-3(t_1-u_1)s_1^{-1}\ln\frac{s}{m^2}$$

$$-(3t_1u_1-6sm^2)s^{-1}u^{-1}\ln\frac{-u_1}{m^2}+(3t_1u_1-6sm^2)s^{-1}t^{-1}\ln\frac{-t_1}{m^2}$$

$$-3(t_1-u_1)s^{-1}\bar{s}^{-1}s_1^{-1}(s^2-8sm^2+8m^4)\left(\zeta(2)+\tfrac{1}{2}\ln^2 x+2\,\mathrm{Li}_2(-x)\right)$$

$$-(3+6us^{-1})\left(-\ln\frac{-u_1}{m^2}\ln\frac{s}{m^2}+\ln^2\frac{-u_1}{m^2}+\mathrm{Li}_2\left(\frac{u}{m^2}\right)\right)$$

$$+(3+6ts^{-1})\left(-\ln\frac{-t_1}{m^2}\ln\frac{s}{m^2}+\ln^2\frac{-t_1}{m^2}+\mathrm{Li}_2\left(\frac{t}{m^2}\right)\right)\Bigg]\delta(s+t_1+u_1)\,, \qquad \text{(A.2)}$$

where A_{QED} and x are defined in eqs. (2.4) and (2.30), respectively. Further we have used the definitions

$$s_1=4m^2-s\,,\qquad \bar{s}=s\sqrt{1-4m^2/s}\,,\qquad \delta=\Delta/m^2\,, \qquad \text{(A.3)}$$

where Δ is defined below eq. (2.20) [see also eq. (2.27)].

A quick glance at the above formulae reveals that the first term of eqs. (A.1) and (A.2) is symmetric under the interchange of t_1 and u_1, whereas the second term is antisymmetric. The above cross sections hold when a heavy antiquark is detected in the final state. Like in sects 2 and 4 the variables t_1 and u_1 always denote the square of the four-momentum transfer of the detected heavy antiquark with respect to the light antiquark and the light quark, respectively If we detect the heavy quark in the final state the production cross sections of the latter are given by the same expressions (A.1) and (A.2) provided the plus sign between the symmetric and antisymmetric part is replaced by a minus sign

Notice that the unrenormalized virtual cross section in eq. (2.8) can be reconstructed from the reduced virtual plus soft expressions in eqs. (A.1), (A.2) and (2.15) in a straightforward way. First we add the Born cross section folded by the splitting function Γ_{qq} in (4 [illegible] 5) to the above expressions. Then subtract the soft cross sections in eqs. (2.28) and (2.29). In this way one obtains the renormalized cross section on the left-hand side of eq. (2.11). The unrenormalized one (with respect to coupling constant renormalization) follows from the right-hand side of the last equation. The abelian (C_F^2) part has already been calculated earlier in the literature in the context of QED corrections to the process $e^+ + e^- \to \mu^+ + \mu^-$ of ref. [30]. To recover the QED expression one should use the splitting function Γ_{qq} where the collinear divergences are regulated by giving the light partons a small mass (on-shell regularization).

Appendix B

Here we present the formulae needed in case one chooses a DIS scheme where the momentum sum rule is preserved Instead of eq (4 18) one chooses

$$f_{\mathrm{gq}}^{\mathrm{DIS}}(x,Q^2,\mu^2) = -f_{\mathrm{qq}}^{\mathrm{DIS}}(x,Q^2,\mu^2), \tag{B.1}$$

where $f_{\mathrm{qq}}^{\mathrm{DIS}}$ is given in eq. (4 5). Hence one has to add the following expressions to eqs (4.23) and (4 24), respectively

$$\Delta\left(s^2\frac{d^2\hat{\sigma}^{(1)}_{g\bar{q},F}}{dt_1\,du_1}\right)^{V+S}_{DIS} = \tfrac{1}{2}\alpha_S^3 K_{gq} N C_F^2\left[\log^2\left(\frac{\Delta}{s+t_1}\right) - \tfrac{3}{2}\log\left(\frac{\Delta}{s+t_1}\right)\right.$$
$$\left. - \tfrac{9}{2} - 2\zeta(2)\right] B_{\mathrm{QED}}\,\delta(s_4), \tag{B.2}$$

$$\Delta\left(s^2\frac{d^2\hat{\sigma}^{(1)}_{g\bar{q},A}}{dt_1\,du_1}\right)^{V+S}_{DIS} = -\tfrac{1}{2}\alpha_S^3 K_{gq} N C_A C_F\left[\left(\frac{t_1u_1}{s^2}\right)\left\{\log^2\left(\frac{\Delta}{s+t_1}\right)\right.\right.$$
$$\left.\left. - \tfrac{3}{2}\log\left(\frac{\Delta}{s+t_1}\right) - \frac{9}{2} - 2\zeta(2)\right\}\right] B_{\mathrm{QED}}\,\delta(s_4), \tag{B.3}$$

with B_{QED} defined in eq. (4.22), and

$$\Delta\left(s^2\frac{d^2\hat{\sigma}^{(1)}_{g\bar{q},F}}{dt_1\,du_1}\right)^{H}_{DIS} = \tfrac{1}{2}\alpha_S^3 K_{gq} N C_F^2\left[\left(-\frac{1}{u_1}\right)\left\{\frac{u_1^2+(s+t_1)^2}{s_4(s+t_1)}\right.\right.$$
$$\left. \times\left(\log\left(\frac{s_4}{-u_1}\right) - \frac{3}{4}\right) + \frac{9}{4} - \frac{5}{4}\frac{u_1}{s+t_1}\right\}$$
$$\left. \times\left\{-\frac{t_1^2+(s+t_1)^2}{t_1(s+t_1)} + \frac{4m^2s}{t_1u_1}\left(1 - \frac{m^2s}{t_1u_1}\right)\right\}\right], \tag{B.4}$$

$$\Delta\left(s^2\frac{d^2\hat{\sigma}^{(1)}_{g\bar{q},A}}{dt_1\,du_1}\right)^{H}_{DIS} = -\tfrac{1}{2}\alpha_S^3 K_{gq} N C_A C_F\left[\left(-\frac{t_1(s+t_1)}{u_1s^2}\right)\left\{\frac{u_1^2+(s+t_1)^2}{s_4(s+t_1)}\right.\right.$$
$$\left. \times\left(\log\left(\frac{s_4}{-u_1}\right) - \frac{3}{4}\right) + \frac{9}{4} - \frac{5}{4}\frac{u_1}{s+t_1}\right\}$$
$$\left. \times\left\{-\frac{t_1^2+(s+t_1)^2}{t_1(s+t_1)} + \frac{4m^2s}{t_1u_1}\left(1 - \frac{m^2s}{t_1u_1}\right)\right\}\right]. \tag{B.5}$$

Also the reduced cross sections calculated in the $\overline{\rm MS}$ scheme for the gluon–gluon fusion process which are presented in eqs. (6.16) and (6.17) of ref. [4] get modified. Here we choose

$$f_{gg}^{\rm DIS}(x,Q^2,\mu^2) = -2n_{\rm f} f_{qg}^{\rm DIS}(x,Q^2,\mu^2) \tag{B.6}$$

Here $n_{\rm f}$ stands for the number of light flavours and $f_{qg}^{\rm DIS}$ is given in eq. (4.19). The expressions in the DIS scheme become

$$\left(s^2\frac{d^2\hat{\sigma}^{(1)}_{gg,\rm O}}{dt_1\,du_1}\right)^{\rm H}_{\rm DIS} = \left(s^2\frac{d^2\hat{\sigma}^{(1)}_{gg,\rm O}}{dt_1\,du_1}\right)^{\rm H}_{\overline{\rm MS}} + \tfrac{1}{4}\alpha_s^3 K_{gg} n_{\rm f} C_{\rm O}\left[\left(-\frac{t_1^2+(s+t_1)^2}{s^2u_1}\right)\right.$$
$$\times\left\{-\frac{8u_1s_4}{(s+t_1)^2}-1+\frac{s_4^2+u_1^2}{(s+t_1)^2}\log\left(\frac{s_4}{-u_1}\right)\right\}$$
$$\left.\times\left\{-\frac{t_1^2+(s+t_1)^2}{t_1(s+t_1)}+\frac{4m^2s}{t_1u_1}\left(1-\frac{m^2s}{t_1u_1}\right)\right\}+(t_1\leftrightarrow u_1)\right], \tag{B.7}$$

$$\left(s^2\frac{d^2\hat{\sigma}^{(1)}_{gg,\rm K}}{dt_1\,du_1}\right)^{\rm H}_{\rm DIS} = \left(s^2\frac{d^2\hat{\sigma}^{(1)}_{gg,\rm K}}{dt_1\,du_1}\right)^{\rm H}_{\overline{\rm MS}} - \tfrac{1}{4}\alpha_s^3 K_{gg} n_{\rm f} C_{\rm K}$$
$$\times\left[\left(-\frac{1}{u_1}\right)\left\{-\frac{8u_1s_4}{(s+t_1)^2}-1+\frac{s_4^2+u_1^2}{(s+t_1)^2}\log\left(\frac{s_4}{-u_1}\right)\right\}\right.$$
$$\left.\times\left\{-\frac{t_1^2+(s+t_1)^2}{t_1(s+t_1)}+\frac{4m^2s}{t_1u_1}\left(1-\frac{m^2s}{t_1u_1}\right)\right\}+(t_1\leftrightarrow u_1)\right]. \tag{B.8}$$

The colour factors appearing in the above expressions are the same as the ones used in ref. [4]:

$$K_{gg} = \frac{1}{(N^2-1)^2}, \qquad C_{\rm O} = N(N^2-1), \qquad C_{\rm K} = \frac{N^2-1}{N} \tag{B.9}$$

Appendix C

In this appendix we discuss the integrations necessary for the calculation of the hadronic differential and total cross sections. The single-particle inclusive hadronic cross section reads [cf. eq. (6.3)]

$$S^2\frac{d^2\sigma(S,T_1,U_1)}{dT_1\,dU_1} = S\frac{d^2\sigma(S,T_1,U_1)}{dp_t^2\,dy}$$

$$= \int_{x_{1-}}^{1}\frac{dx_1}{x_1}\int_{x_{2-}}^{1}\frac{dx_2}{x_2}H_{ij}(x_1,x_2,Q^2)s^2\frac{d^2\hat{\sigma}_{ij}(s,t_1,u_1)}{dt_1\,du_1}. \quad (C\,1)$$

The hadronic invariants S, T_1, U_1, and their partonic analogues s, t_1, u_1 were defined in sect. 6 If $t_1 = x_1 T_1$ and $u_1 = x_2 U_1$ then the lower limits x_{1-}, x_{2-} are defined by [see also eq. (6 5)],

$$x_{1-} = \frac{-U_1}{S+T_1}, \qquad x_{2-} = \frac{-x_1 T_1}{x_1 S + U_1} \quad (C\,2)$$

The rapidity and transverse momentum of the produced heavy (anti-)quark are denoted by (the lower case letters) y and p_t, respectively The rapidity is defined by $y = \frac{1}{2}\ln(T_1/U_1)$ Note that the transverse momentum squared $p_t^2 = t_1 u_1/s - m^2 = T_1 U_1/S - m^2$ is invariant under boosts along the beam direction

Denoting the Born cross sections (1 2) and (1.3) by the following shorthand notation

$$s^2\frac{d^2\hat{\sigma}_{ij}^{(0)}}{dt_1\,du_1} = \delta(s+t_1+u_1)\sigma_{ij}^{(0)}(s,t_1,u_1), \quad (C\,3)$$

their contributions to the hadronic cross section (C.1) can be written as

$$\left(S\frac{d^2\sigma(S,T_1,U_1)}{dp_t^2\,dy}\right)^{B} = \int_{x_{1-}}^{1}\frac{dx_1}{x_1}\left(-\frac{1}{x_1 T_1}\right)H_{ij}\left(x_1, -\frac{x_1 T_1}{x_1 S+U_1}, Q^2\right)$$

$$\times\,\sigma_{ij}^{(0)}\left(-\frac{x_1^2 T_1}{x_1 S+U_1}S,\; x_1 T_1,\; -\frac{x_1 T_1}{x_1 S+U_1}U_1\right), \quad (C\,4)$$

with x_{1-} given by (C.2).

The order α_s correction to the hadronic cross section is split into a soft plus virtual (S + V) and a hard (H) gluon piece. The hard gluon piece of the hadronic cross section reads

$$\left(S\frac{d^2\sigma(S,T_1,U_1)}{dp_t^2\,dy}\right)^H = \int_{x_1^-}^1 \frac{dx_1}{x_1}\int_{x_2^*}^1 \frac{dx_2}{x_2} H_{ij}(x_1,x_2,Q^2)$$

$$\times\left(s^2\frac{d^2\hat{\sigma}_{ij}^{(1)}}{dt_1\,du_1}(x_1x_2S,x_1T_1,x_2U_1)\right)^H, \qquad (C.5)$$

where x_{2-}^* is determined by the condition

$$s_4 = x_1x_2S + x_1T_1 + x_2U_1 > \Delta\,, \qquad (C.6)$$

which yields

$$x_{2-}^* = (\Delta - x_1T_1)/(x_1S + U_1)\,. \qquad (C.7)$$

For the actual integrations it is convenient to change variables from x_2 to s_4 with the limits $\Delta < s_4 < s_4^{max} \equiv x_1(S+T_1) + U_1$.

$$\int_{x_2^*}^1 \frac{dx_2}{x_2} = \int_\Delta^{s_4^{max}} \frac{ds_4}{s_4 - x_1T_1} \qquad (C.8)$$

The soft plus virtual piece is evaluated with elastic kinematics so that $s_4 = 0$. Thus its contributions are proportional to $\delta(s_4)$ and can be denoted by

$$\left(s^2\frac{d^2\hat{\sigma}_{ij}^{(1)}}{dt_1\,du_1}\right)^{V+S} = \delta(s+t_1+u_1)(\sigma_{ij})^{V+S}(s,t_1,u_1,\Delta)\,. \qquad (C.9)$$

The soft plus virtual piece of the hadronic cross section equals

$$\left(S\frac{d^2\sigma(S,T_1,U_1)}{dp_t^2\,dy}\right)^{V+S} = \int_{x_1^-}^1 \frac{dx_1}{x_1}\left(-\frac{1}{x_1T_1}\right)H_{ij}\left(x_1,-\frac{x_1T_1}{x_1S+U_1},Q^2\right)$$

$$\times\sigma_{ij}^{V+S}\left(-\frac{x_1^2T_1}{x_1S+U_1}S, x_1T_1, -\frac{x_1T_1}{x_1S+U_1}U_1,\Delta\right). \qquad (C.10)$$

In our numerical program we rewrite the $\ln^i(\Delta)$ $(i = 0,1,2)$ terms in $(\sigma_{ij})^{V+S}(s,t_1,u_1,\Delta)$ into integrations over s_4

$$(\sigma_{ij})^{V+S}(s,t_1,u_1,\Delta) \equiv \sum_{k=0}^{2} a_k \ln^k(\Delta/m^2)$$

$$= \sum_{k=0}^{2} a_k \int_\Delta^{s_4^{max}} \frac{ds_4}{s_4^{max}-\Delta} A_k \qquad (C.11)$$

with certain coefficients α_k. In this way the S + V piece and the H piece can directly be added The result is a flat s_4 distribution for the total order α_S corrections $(d\sigma)^{H+S+V}$ and the lower limit Δ can be put to zero The quantities A_k in (C 11) are given by

$$A_0 = 1\,,$$

$$A_1 = \ln\left(\frac{s_4^{\max}}{m^2}\right) - \frac{s_4^{\max} - \Delta}{s_4}\,,$$

$$A_2 = \ln^2\left(\frac{s_4^{\max}}{m^2}\right) - 2\frac{s_4^{\max} - \Delta}{s_4}\ln\left(\frac{s_4}{m^2}\right). \tag{C 12}$$

The total cross section can be derived by integrating $(d\sigma)^{B}$ and $(d\sigma)^{H+V+S}$ over the variables p_t^2 and y with the appropriate limits

$$\int_{m^2}^{S/4} dm_t^2 \int_{-(\cosh^{-1}\sqrt{S})/2m_t}^{(\cosh^{-1}\sqrt{S})/2m_t} dy = \int_{-\frac{1}{2}\ln[(1+\beta)/(1-\beta)]}^{\frac{1}{2}\ln[(1+\beta)/(1-\beta)]} dy \int_{m^2}^{S/(4\cosh^2 y)} dm_t^2$$

$$= \int_{-1}^{1} dx_F \int_{m^2}^{S/4-p_L^2} dm_t^2\, \frac{\sqrt{S-4m^2}}{2m_t \cosh y}\,, \tag{C 13}$$

where $\beta = \sqrt{(1-4m^2/S)}$ and $m_t = \sqrt{m^2+p_t^2}$ In each case

$$T_1 = -\sqrt{S}\, m_t \exp(y)\,, \qquad U_1 = -\sqrt{S}\, m_t \exp(-y)\,. \tag{C 14}$$

The second line in eq (C 13) was used for the x_F distributions Here x_F is defined in the (hadronic) c.m. frame, $x_F = p_L/p_L^{\max}$, where the maximal longitudinal heavy quark momentum is given by $p_L^{\max} = \sqrt{S/4 - m^2}$ Finally, the rapidity y is related to p_L via $p_L = m_t \sinh y$

References

[1] M Gluck, J F Owens and E Reya, Phys Rev D15 (1978) 2324,
B L Combridge, Nucl Phys B151 (1979) 429
[2] P Nason, S Dawson and R K Ellis, Nucl Phys B303 (1988) 607
[3] P. Nason, S Dawson and R.K Ellis, Nucl Phys B327 (1989) 49
[4] W Beenakker, H. Kuijf, W L van Neerven and J Smith, Phys Rev D40 (1989) 54
[5] P. Sinervo 1989 Int Symposium on Lepton-photon interactions at high energy Stanford CA
F. Abe et al , Phys Rev Lett 64 (1990) 142, 147
[6] K. Eggert, 1989 Int Symposium on Lepton- photon interactions at high energy, Stanford, CA
[7] L. Di Lella, 1989 Int Symposium on Lepton–photon interactions at high energy, Stanford, CA
[8] C Albajar et al , (UA1 experiment) Phys Lett B213 (1988) 405

[9] R. Meng, G.A. Schuler, J. Smith and W.L. van Neerven, Nucl. Phys. B339 (1990) 325
[10] ISAJET: F. Paige and S. Protopopescu, Brookhaven report BNL-38034 (1986)
[11] EUROJET: A. Ali, B. van Eijk and I. ten Have, Nucl. Phys. B292 (1987) 1
[12] HERWIG: G. Marchesini and B.R. Webber, Cambridge preprint Cavendish-HEP-88/7 (1988); Nucl. Phys. B330 (1990) 261
[13] T. Matsuura, S.C. van der Marck and W.L. van Neerven, Phys. Lett. B211 (1988) 171; Nucl. Phys. B319 (1989) 570.
[14] J. Smith, D. Thomas and W.L. van Neerven, Z. Phys. C44 (1989) 267
[15] A. P. Contogouris, S. Papadopoulos and J.P. Ralston, Phys. Lett. B104 (1981) 70; Phys. Rev. D24 (1982) 1280;
A.P. Contogouris, N. Mebarki and S. Papadopoulos, The dominant part of the higher order corrections in perturbative QCD, McGill preprint;
A.P. Contogouris and S. Papadopoulos, The dominant part of the higher order corrections for the process $q + g \to \gamma + q$, McGill preprint
[16] G. Passarino and M. Veltman, Nucl. Phys. B160 (1979) 151
[17] W.J.P. Beenakker, Electroweak corrections: techniques and applications, Ph.D. thesis, University of Leiden, The Netherlands (1989)
[18] R.K. Ellis and J.C. Sexton, Nucl. Phys. B269 (1986) 445
[19] J. Kubar André and F.E. Paige, Phys. Rev. D19 (1978) 221;0
B. Humpert and W.L. van Neerven, Nucl. Phys. B184 (1981) 221;
[20] R. Lewin, Polylogarithms and Associated Functions (North-Holland, Amsterdam, 1983)
[21] E.G. Floratos, D.A. Ross and C.T. Sachrajda, Nucl. Phys. B129 (1977) 66 [Erratum B139 (1978) 545], B152 (1979) 493;
A. Gonzales-Arroyo, C. Lopez and F.J. Yndurain, Nucl. Phys. B153 (1979) 161;
A. Gonzales-Arroyo and C. Lopez, Nucl. Phys. B166 (1980) 429;
E.G. Floratos, P. Lacaze and C. Kounnas, Phys. Lett. B98, (1981) 89, 285
[22] V.N. Gribov and L.N. Lipatov, Sov. J. Nucl. Phys. 15 (1972) 438, 675;
G. Altarelli and G. Parisi, Nucl. Phys. B126 (1977) 298
[23] G. Altarelli, R.K. Ellis and G. Martinelli, Nucl. Phys. B157 (1979) 461
[24] A.N.J.J. Schellekens, Perturbative QCD and Lepton Pair Production, Ph.D. thesis, Nijmegen University, The Netherlands (1981)
[25] A.H. Mueller and P. Nason, Phys. Lett. B156 (1985) 226; Nucl. Phys. B266 (1986) 265
[26] M. Diemoz, F. Ferroni, E. Longo and G. Martinelli, Z. Phys. C39 (1988) 472
[27] G. Altarelli, M. Diemoz, G. Martinelli and P. Nason, Nucl. Phys. B308 (1988) 724
[28] Talk by S. McMahon (UA1 experiment) at the XXVth Rencontres de Moriond, Les Arcs (March 1990)
[29] J.F. Owens, Phys. Rev. D30 (1984) 943
[30] F.A. Berends, K.J.F. Gaemers and R. Gastmans, Nucl. Phys. B57 (1973) 381; B63 (1973) 381;
D.Yu. Bardin, M.S. Bilenky, O.M. Fedorenko and T. Riemann, Dubna Preprint E2-88-324 (1988)